National Defence / Défense nationale

THEORETICAL BIT ERROR RATE PERFORMANCE OF THE KALMAN FILTER EXCISOR FOR FM INTERFERENCE

by

Brian Kozminchuk

DEFENCE RESEARCH ESTABLISHMENT OTTAWA
REPORT NO. 1163

Canada

December 1992
Ottawa

National Defence / Défense nationale

THEORETICAL BIT ERROR RATE PERFORMANCE OF THE KALMAN FILTER EXCISOR FOR FM INTERFERENCE

by

Brian Kozminchuk
Communications Electronic Warfare Section
Electronic Warfare Division

DEFENCE RESEARCH ESTABLISHMENT OTTAWA
REPORT NO. 1163

PCN
041LK11

December 1992
Ottawa

ABSTRACT

This technical report develops a theoretical bit error rate expression for a Kalman filtering technique that is used for filtering narrowband interferers out of direct sequence spread spectrum signals. The approach is based on the digital phase-locked loop Kalman filter and is close to optimum in so far as demodulating an FM-type of interferer. Because the interference is assumed to be much stronger than either the signal or noise, the Kalman filter locks onto the interference and produces estimates of its phase and envelope. Several assumptions are made in the development of the theoretical bit error rate expression and these are expanded upon. It is shown and illustrated that theory agrees well with simulation as long as the bandwidth of the low pass filter used to determine the envelope of the interference is much less than the sampling rate, otherwise the interference estimate at the input to the interference canceller will have significant cross-correlation with the signal, leading to some cancellation of the spread spectrum signal.

RÉSUMÉ

Ce rapport élabore une expression mathématique donnant le taux d'erreur de bits quand un filtrage de Kalman est utilisée pour la suppression d'interférences sur des signaux à spectre étalé par séquence directe. L'approche repose sur un filtre de Kalman asservi numériquement par verrouillage de phase et s'avère quasi-optimum quant à la démodulation d'une interférence de type MF. Puisqu'on présuppose que l'interférence est plus forte le signal ou que le bruit, le filtre de Kalman se verrouille sur l'interférence et permet l'estimation de sa phase et de son enveloppe. On élabore sur la nature des hypothèses qui doivent être posées lors du développement de l'expression gouvernant le taux d'erreur de bits. On démontre éloquemment que la théorie est en parfait accord avec les simulations tant que la largeur de bande du filtre passe-bas, servant à circonscrire l'enveloppe de l'interférence, est inférieure au taux d'échantillonnage. Autrement, l'estimation de l'interférence, à l'entrée même où elle doit être cancellée, sera affectée de façon importante par des intercorrélations avec le signal, amenant un évanouissement partiel du signal à spectre étalé.

EXECUTIVE SUMMARY

This technical report develops a theoretical bit error rate expression for a Kalman filtering technique that is used for filtering narrowband interferers out of direct sequence spread spectrum signals. These signals are used extensively in military communication systems. The technique described herein applies equally to both Electronic Support Measures (ESM) systems and direct sequence spread spectrum communication sytems. In the former application, the ESM system may be attempting to intercept the spread spectrum signal, but the narrowband interference may be hampering this effort. In the latter application, the spread spectrum communication system may require additional assistance to suppress the interference. Since the open literature has been devoted to this latter case, the material presented here focuses on the communications application.

One of the attributes of direct sequence spread spectrum communication systems is their ability to combat interference or intentional jamming by virtue of the system's processing gain inherent in the spreading and despreading process. The interference can be attenuated by a factor as high as this processing gain. In some cases, however, the gain is insufficient to effectively suppress the interferer, leading to a significant degradation in communications manifested by an increase in bit error rate. If the ratio of interference bandwidth to spread spectrum bandwidth is small, the interference can be filtered out to enhance system performance. However, this is at the expense of introducing some distortion onto the signal. This process of filtering is sometimes referred to as interference excision.

The Kalman filtering approach to excision is based on the digital phase-locked loop Kalman filter which is close to optimum in a minimum mean-squared error sense for demodulating an FM interferer. Because the interference is assumed to be much stronger than either the signal or noise, the Kalman filter locks onto the interference and produces an estimate of the phase and envelope of the interference.

Several assumptions are made in the development of the theoretical bit error rate expression and these are expanded upon. It is shown mathematically and illustrated that theory agrees well with simulation as long as the bandwidth of the low pass filter used to determine the envelope of the interference is much less than the sampling rate. If this condition is not met, then the interference estimate at the input to the interference canceller will have significant cross-correlation with the signal, leading to a certain degree of signal cancellation.

TABLE OF CONTENTS

LIST OF TABLES

LIST OF FIGURES

1.0 INTRODUCTION

The problem of interference suppression in direct sequence spread spectrum communications sytems is well-known [2, 3, 4, 5].

A suppression technique based on the Kalman filter was presented in [6]. There, a function related to the interference is assumed to have been generated by a second order nonlinear state-space system to which the extended Kalman filter equations are applied. This results in what has been termed the digital phase-locked loop (DPLL) [1, 7]. This approach to interference suppression is close to optimum for the suppression of constant envelope or FM-types of interferers and, therefore, can potentially provide better performance than the recursive least squares (RLS) algorithm which was analyzed for the swept tone in [5, 8].

The objective of this technical report is to derive a theoretical equation describing the bit error rate performance of the DPLL and to compare this theoretical expression to simulated results. The interference is assumed to be of the FM-type generated by the state-space model defined in [6, 1].

The outline of this technical report is as follows. Section 2.0 describes the spread spectrum communications model. Section 3.0 details the interference model used in generating the interference and the Kalman algorithm. Section 4.0 presents the interference estimator. Section 5.0 develops the theoretical bit error rate equation. This expression is compared to simulated results. Finally, Section 6.0 concludes the technical report, suggesting areas for further research.

2.0 COMMUNICATIONS MODEL

The basic elements of the BPSK PN spread spectrum receiving system are shown in Fig. 1. The received waveform $r(t)$, consisting of a spread spectrum signal, additive white Gaussian noise, and narrowband interference is applied to a bandpass filter with the transfer function $H_{bp}(f)$, whose output is defined as

$$u(t) = s(t) + n(t) + i(t). \tag{1}$$

The bandpass filter $H_{bp}(f)$, for the application considered here, is assumed to be a filter matched to a chip and centered at the angular carrier frequency ω_0 of the spread spectrum signal. The spread spectrum signal is defined as

$$s(t) = a(t)\cos(\omega_0 t) \tag{2}$$

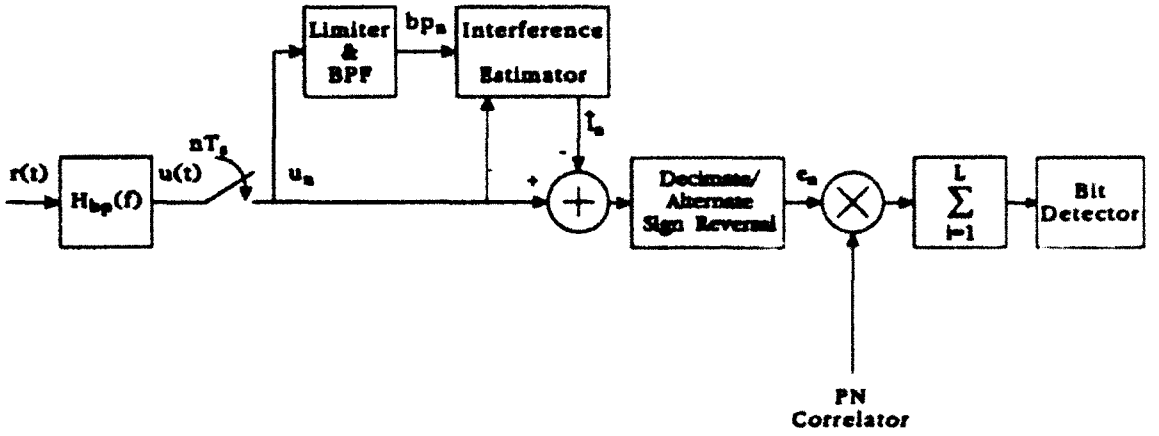

Figure 1: Spread spectrum communications model.

where

$$a(t) = \sum_k D_k b_k(t - kT_b). \tag{3}$$

In Eq. (3), D_k is a sequence of data bits of amplitude (± 1) and duration T_b seconds (bit rate $R_b = 1/T_b$), and $b_k(t - kT_b)$ is the PN sequence pattern for the k^{th} bit, i.e.,

$$b_k(t) = \sum_{j=1}^{L} c_{kj} q(t - jT_c) \tag{4}$$

with L being the number of pseudo random chips per bit, or the processing gain, c_{kj} is the code sequence for the bit, $q(t)$ representing the basic chip pulse of energy E_c, and T_c the reciprocal of the chip rate R_c.

The noise $n(t)$ is Gaussian and has a power spectral density

$$S_n(f) = \frac{N_0}{2} |H_{bp}(f)|^2, \tag{5}$$

where $N_0/2$ is the power spectral density of the assumed white Gaussian noise from the channel. The band of interference is defined as

$$i(t) = I(t) \cos(\omega_0 t + \theta(t)) \tag{6}$$

where $I(t)$ is the interference amplitude and $\theta(t)$ is the phase modulation. It has been assumed that the effect of the bandpass filter $H_{bp}(f)$ is negligible on the interference $i(t)$. This would not be true in reality, since the bandpass filter will induce some amplitude modulation on the constant envelope interference. The rate of change of the envelope

would therefore depend on the rate of change of the instantaneous frequency, and the amplitude deviation would depend on the frequency offset from ω_0 and the interference bandwidth. The fact that this report considers the amplitude to be of constant envelope at the output of the bandpass filter corresponds to the best case situation.

Referring to Fig. 1, the output $u(t)$ of the bandpass filter $H_{bp}(f)$ is bandpass sampled and applied to a limiter/bandpass filter and interference estimator.

Consider the bandpass sampler first. The analog signal $u(t)$ from Eq. (1) is sampled at $f_s = 2R_c$ ($mf_s = \omega_0/2\pi + R_c/2$ for some integer m). The resultant sampled signal is, therefore,

$$u_n = s_n + n_n + i_n, \tag{7}$$

where s_n consists of the sequence $\{\ldots, 0, (-1)^n a_n, 0, (-1)^{n+2} a_{n+2}, \ldots\}$ where the a_n are of energy E_c and coded according to $c_{kj} D_k$ for the j^{th} chip in the k^{th} transmitted bit, n_n [1] are uncorrelated Gaussian noise samples of variance $\sigma^2_{nse} = E_c(N_0/2)$, and i_n is the sampled version of Eq. (6). The samples u_n are applied to the interference estimator and interference canceller.

The interference estimator produces an estimate $\hat{i}_n$ of the interference which is removed from the sampled input u_n. The output of the summer is decimated and sign-reversed, resulting in a baseband error signal e_n. This error signal is correlated with the PN sequence. The output of the correlator is integrated and bit-detected.

3.0 INTERFERENCE MODEL AND KALMAN ALGORITHM

This section presents the state-space models of the interference. The development here follows that in [1].

A block diagram of the analog state space model which generates the analog version of a function related to bp_n in Fig. 1 is shown in Fig. 2; this function is represented by $bp(t)'$. The state-space equations are defined as

$$\begin{bmatrix} \dot{x}_1(t) \\ \dot{x}_2(t) \end{bmatrix} = \begin{bmatrix} 0 & d \\ 0 & -\alpha \end{bmatrix} \begin{bmatrix} x_1(t) \\ x_2(t) \end{bmatrix} + \begin{bmatrix} 0 \\ \sqrt{K_w} \end{bmatrix} w(t), \tag{8}$$

where $x_1(t)$ and $x_2(t)$ are the phase function and modulating signal state variables of the

[1] Coherent bandpass sampling has been assumed, so that the in-phase component is $(n_{1,n}/\sqrt{2})\cos(n\pi/2)$ and the quadrature component is $(n_{2,n}/\sqrt{2})\sin(n\pi/2)$

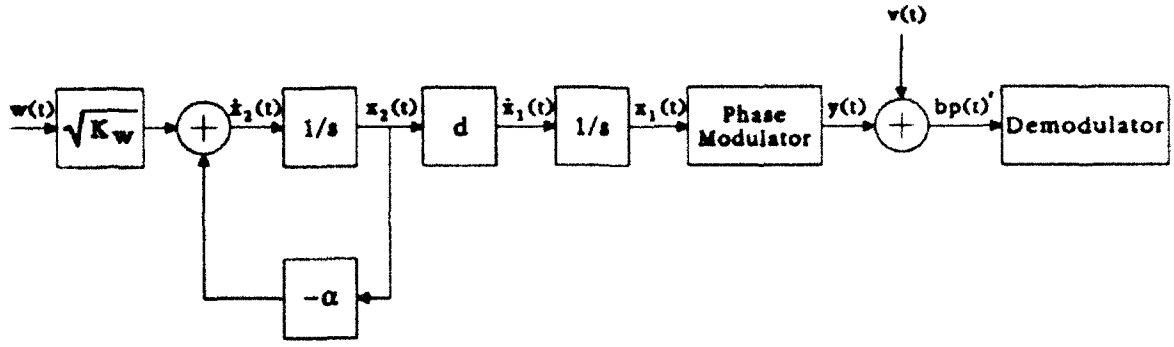

Figure 2: Block diagram of the state space model.

interference, respectively. In compact form Eq. (8) becomes

$$\dot{\boldsymbol{x}}(t) = \boldsymbol{A}\boldsymbol{x}(t) + \boldsymbol{g}w(t). \tag{9}$$

The interferer's modulating signal $x_2(t)$ is assumed to be generated by applying Gaussian white noise, $w(t)$, of unit variance to an amplifier with gain $\sqrt{K_w}$ followed by a first order low pass filter of bandwidth $\alpha = 2\pi\alpha_f$. The steady state variance of the coloured noise at the output of the lowpass filter is unity if $K_w = 2\alpha$. The output is multiplied by the frequency deviation constant, d, and then integrated to yield the phase function

$$x_1(t) = d\int_0^t x_2(\tau)\,d\tau. \tag{10}$$

An FM type of signal (interferer) is generated by phase modulating a carrier, ω_0, which has been set equal to the carrier of the spread spectrum signal, since any offsets from ω_0 can be incorporated into $x_1(t)$, yielding

$$y(t) = \sqrt{2}\cos[\omega_0 t + x_1(t)]. \tag{11}$$

This signal is corrupted by white Gaussian noise $v(t)$ with power spectral density $N_{obs}/2$, generally different from $N_0/2$ defined earlier for the communications model in Fig. 1. The result is an FM signal defined as

$$bp(t)' = y(t) + v(t). \tag{12}$$

Given the observation process $bp'(t)$ from Eq. (12), the objective is to estimate the state $x_1(t)$ and the related state $x_2(t)$, as well as $y(t)$ in Eq. (11). One approximate technique reserved for nonlinear estimation problems [9] is the extended Kalman filter

algorithm.

Before the algorithm is presented, the discrete forms of Eqs. (8) and (9) will be stated, namely,

$$\boldsymbol{x}_{n+1} = \boldsymbol{\phi}\boldsymbol{x}_n + \boldsymbol{w}_n, \tag{13}$$

where n represents discrete time,

$$\boldsymbol{\phi} = \begin{bmatrix} 1 & \beta(1 - e^{-\alpha T_s}) \\ 0 & e^{-\alpha T_s} \end{bmatrix} = \begin{bmatrix} 1 & \phi_{12} \\ 0 & \phi_{22} \end{bmatrix} \tag{14}$$

and

$$\boldsymbol{w}_n = \int_{nT_s}^{(n+1)T_s} \boldsymbol{\phi}\boldsymbol{g}\boldsymbol{w}(z)\, dz. \tag{15}$$

In Eq. (14), $\beta = d/\alpha$ and is termed the bandwidth expansion ratio in units of $volts^{-1}$ [10] and T_s is the sampling interval. In Eq. (15), $\boldsymbol{w}_n$ is a stationary zero-mean white Gaussian vector sequence whose covariance, (i.e., $E\{\boldsymbol{w}_n\boldsymbol{w}_n^t\}$ where the superscript t refers to the matrix transpose), is given by

$$\boldsymbol{V}_w = \int_{nT_s}^{(n+1)T_s} \boldsymbol{\phi}\boldsymbol{g}\boldsymbol{g}^t\boldsymbol{\phi}\, du. \tag{16}$$

Finally, Eq. (12) becomes,

$$bp'_n = y_n + v_n, \tag{17}$$

where y_n is the sampled version of Eq. (11), i.e.,

$$y_n = \sqrt{2}\cos(\omega_0 n T_s + x_{1,n}). \tag{18}$$

It has been assumed that $bp'(t)$ from Eq. (12) has been applied to a bandpass filter of bandwidth B, whose output has been sampled at a rate so as to yield uncorrelated noise samples v_n of variance $\sigma_v^2 = B(N_{obs}/2)$ [7]. It should be noted that bp'_n in Eq. (17) is closely related to bp_n in Fig. 1. The difference is due to the fact that in bp_n, as shown later, the noise is not additive as in Eq. (17), but is contained in the argument of the cosine function of y_n in Eq. (18) due to the hardlimiting process. For large interference-to-signal-plus-noise conditions, however, the effect of the additive noise in Eq. (17) will be similar; thus this model is valid.

The noise covariance matrix, $\boldsymbol{V}_w$, is obtained by substituting Eq. (14) and $\boldsymbol{g}$

from Eq. (9) into Eq. (16) and integrating each term, yielding

$$V_w = \frac{K_w}{2\alpha}\begin{bmatrix} \beta^2\left(4\pi/\gamma - 3 + 4e^{-2\pi/\gamma} - e^{-4\pi/\gamma}\right) & \beta\left(1 - e^{-2\pi/\gamma}\right) \\ \beta\left(1 - e^{-2\pi/\gamma}\right) & 1 - e^{-4\pi/\gamma} \end{bmatrix} \tag{19}$$

where $\gamma = 2\pi/(\alpha T_s)$, which is the ratio of the sampling rate $f_s = 1/T_s$ to the interferer's modulating signal bandwidth α_f. The discrete form of the interference model is shown in Fig. 3.

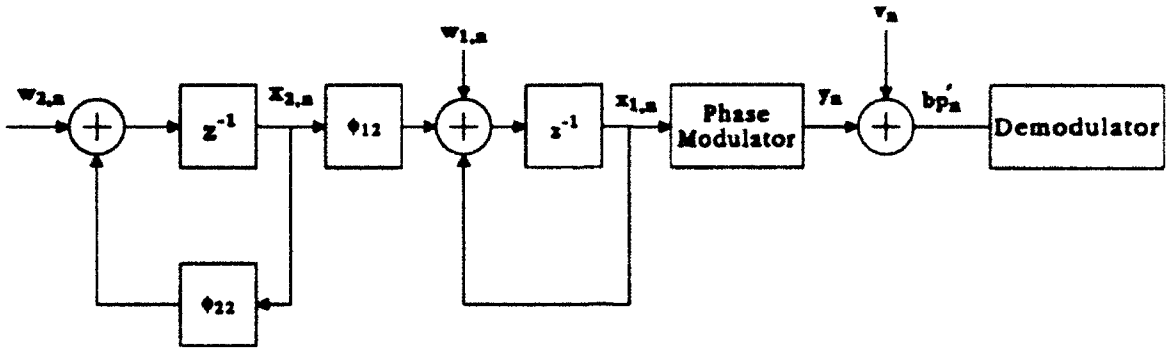

Figure 3: Discrete form of the interference model.

The demodulator in Fig. 3 is the Kalman filter algorithm listed in Table 1 [6, 1]. In the algorithm $\hat{\boldsymbol{x}}_n$ is defined as the estimate of the true state vector $\boldsymbol{x}_n$, $\tilde{\boldsymbol{x}}_n$ is defined as the post error $\boldsymbol{x}_n - \hat{\boldsymbol{x}}_n$, $\boldsymbol{K}_n$ is the Kalman gain vector, $\boldsymbol{V}_{\tilde{x}_n} = E\{\tilde{\boldsymbol{x}}_n\tilde{\boldsymbol{x}}_n^t\}$ is the post error covariance and $\boldsymbol{V}_{\tilde{x}_{n|n-1}} = E\{\tilde{\boldsymbol{x}}_{n|n-1}\tilde{\boldsymbol{x}}_{n|n-1}^t\}$ is the prior error covariance. Furthermore, $f_{n|n-1}^{-1}$ is known as the "coupled equation", since the estimate of the interferer's phase is contained in it. However, this equation can be further approximated as noted in [1]. The approximation is

$$f_{n|n-1}^{-1} \approx \frac{1}{V_{\tilde{x}_{11,n|n-1}}}\left\{1 - \sqrt{\frac{\sigma_v^2}{\sigma_v^2 + V_{\tilde{x}_{11,n|n-1}}}}\right\}. \tag{20}$$

The block diagram of this demodulator is illustrated in Fig. 4 (also referred to as the digital phase-locked loop or DPLL). It produces an estimate of the phase $\hat{x}_{1,n|n-1} = \hat{\theta}_{n|n-1}$ and a signal in quadrature to y_n in Eq. (18); this signal, defined as

$$VCO_n = -\sqrt{2}\sin(\omega_0 n T_s + \hat{\theta}_{n|n-1}), \tag{21}$$

is analogous to the voltage-controlled oscillator (VCO) signal of a phase-locked loop.

Performance curves of the demodulator can be obtained [1] using the baseband simulation model with unit sampling interval, i.e., $T_s = 1$ or $f_s = 1$ Hz. A few examples

Table 1: The Kalman Filter Algorithm.

Initial Conditions:

$$\hat{\boldsymbol{x}}_{-1} = E\{\hat{\boldsymbol{x}}_{-1}\} = \begin{bmatrix} m_1 \\ m_2 \end{bmatrix}; \qquad \boldsymbol{V}_{\tilde{x}_{-1}} = E\{\tilde{\boldsymbol{x}}_{-1}\tilde{\boldsymbol{x}}_{-1}^t\}$$

Do for $n = 0$ to T:

$$\hat{\theta}_{n|n-1} = \begin{bmatrix} 1 & 0 \end{bmatrix} \boldsymbol{\phi}\hat{\boldsymbol{x}}_{n-1}$$

$$\boldsymbol{V}_{\tilde{x}_{n|n-1}} = \boldsymbol{\phi}\boldsymbol{V}_{\tilde{x}_{n-1}}\boldsymbol{\phi}^t + \boldsymbol{V}_w$$

$$f_{n|n-1}^{-1} = \frac{1 - \cos(2\omega_0 n + 2\hat{\theta}_{n|n-1})}{\sigma_v^2 + V_{\tilde{x}_{11},n|n-1}\left[1 - \cos(2\omega_0 n + 2\hat{\theta}_{n|n-1})\right]}$$

$$\boldsymbol{V}_{\tilde{x}_n} = \boldsymbol{V}_{\tilde{x}_{n|n-1}} - \boldsymbol{V}_{\tilde{x}_{n|n-1}} \begin{bmatrix} 1 & 0 \\ 0 & 0 \end{bmatrix} \boldsymbol{V}_{\tilde{x}_{n|n-1}} f_{n|n-1}^{-1}$$

$$\boldsymbol{K}_n = -\boldsymbol{V}_{\tilde{x}_n} \begin{bmatrix} 1/\sigma_v^2 \\ 0 \end{bmatrix} \sqrt{2}\sin(\omega_0 n + \hat{\theta}_{n|n-1})$$

$$\hat{\boldsymbol{x}}_n = \boldsymbol{\phi}\hat{\boldsymbol{x}}_{n-1} + \boldsymbol{K}_n\left[bp'_n - \sqrt{2}\cos(\omega_0 n + \hat{\theta}_{n|n-1})\right]$$

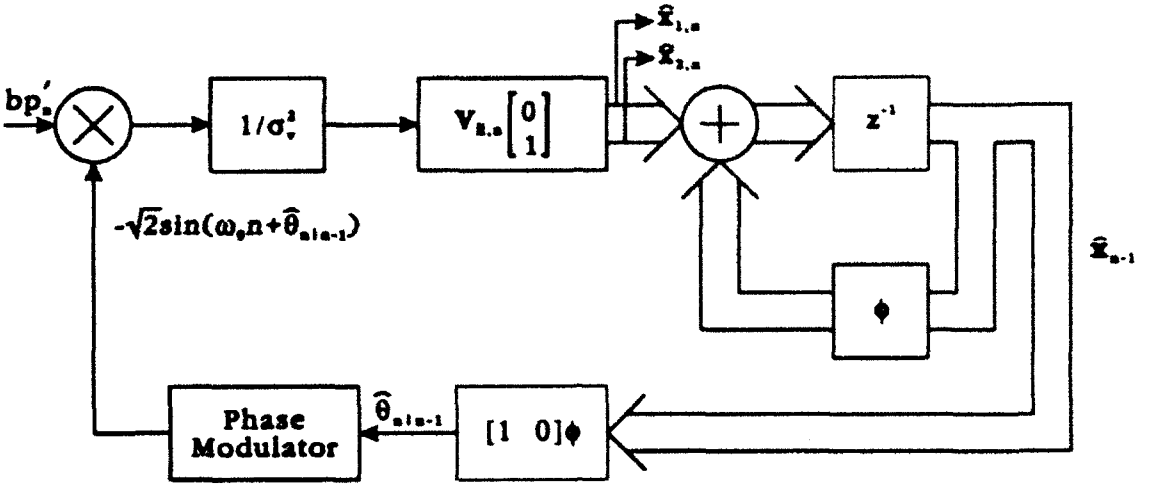

Figure 4: State space representation of the DPLL.

will now be presented.

The theoretical performance curves were obtained using the prior error covariance equation in Table 1 (i.e., $V_{\tilde{x}_{n|n-1}}$). The experimental curves were obtained using the model in Fig. 3 for a range of values for d and σ_v^2; α_f was fixed at 0.0003125 Hz. The results are illustrated in Figs. 5 and 6 and refer to the *filter* form of the Kalman algorithm which is listed in Table 1. The modified Kalman algorithm, which is similar (except for the definitions in ϕ and V_w), is described in [6].

The results are illustrated in Figs. 5 and 6 and indicate reasonable agreement between theory and simulation. It must be pointed out that the theory does not predict the threshold at which the variance of the phase-noise increases dramatically; this must be determined from experimentation. As cited in [1], an approximate threshold is a phase variance of 0.25 radians^2/second^2, (i.e., $1/V_{x_{11,\infty}} = 4$). The results for the modified Kalman algorithm as shown in Fig. 6 exhibit a higher threshold. Otherwise, from the perspective of phase-noise variance, the two algorithms perform almost identically.

4.0 INTERFERENCE ESTIMATOR

Referring to Fig. 1, consider the branch containing the limiter. Here, u_n is applied to a limiter/bandpass filter. The input to the limiter referenced to the interference is redefined as

$$u_n = \sqrt{[I_n + n'_{1,n} + a'_{1,n}]^2 + [n'_{2,n} + a'_{2,n}]^2}\cos(\omega_0 n + \theta_n + \phi_{u,n}) \qquad (22)$$

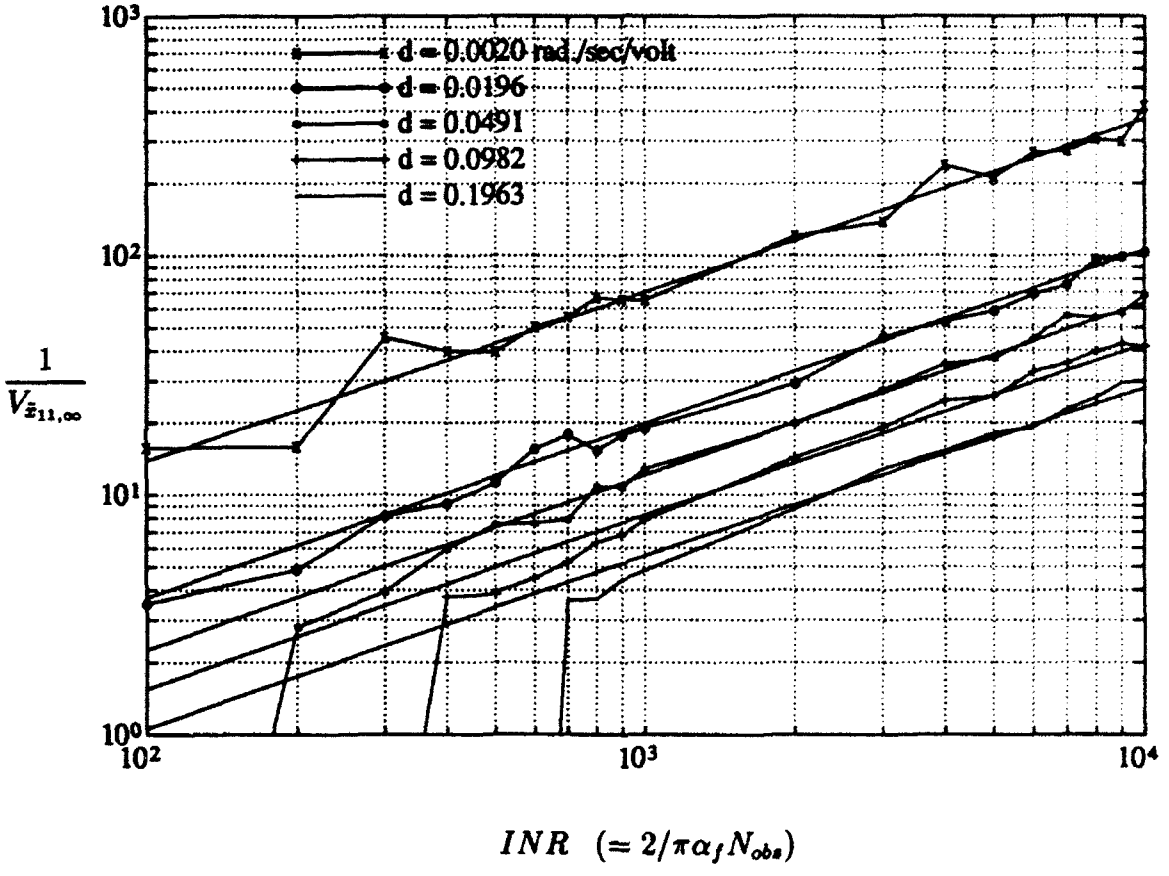

Figure 5: Performance curves using the model in [1] for the case when the Kalman filter is in the filter mode.

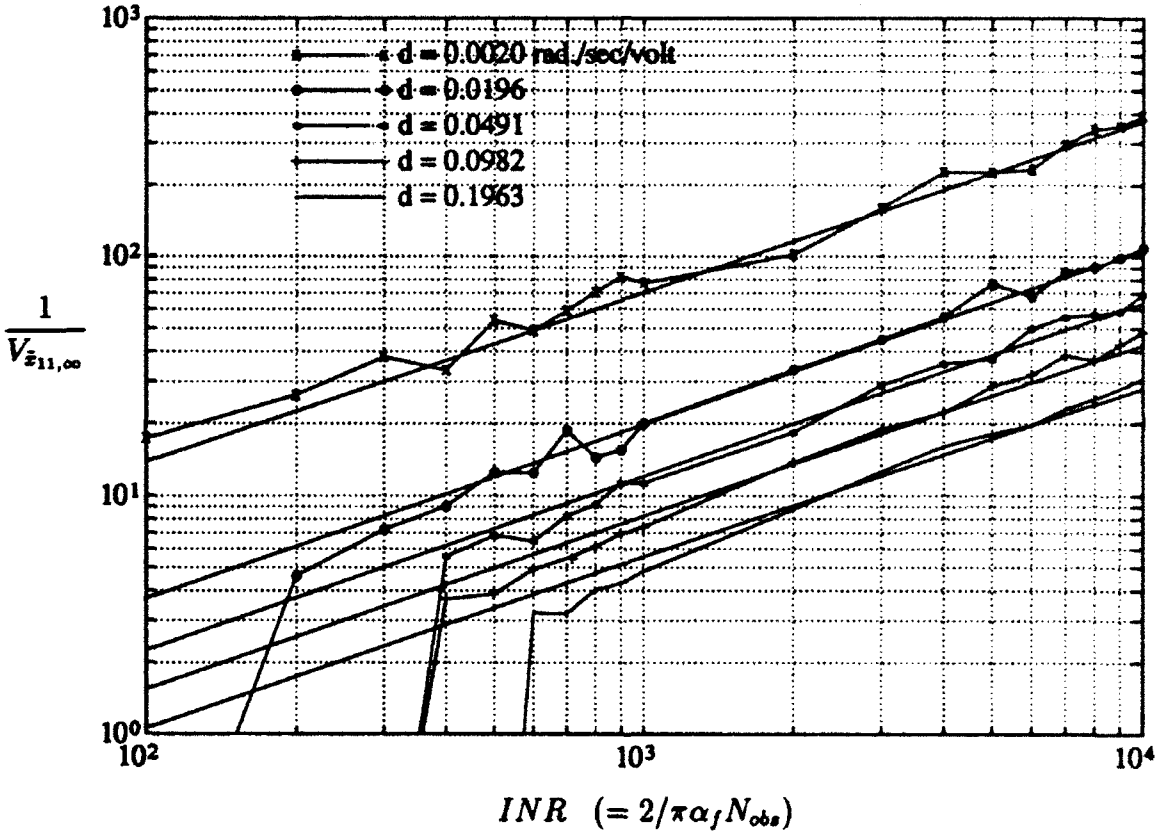

Figure 6: Performance curves using the modified Kalman filter in the filter mode.

where

$$\phi_{u,n} = \arctan\left(\frac{n'_{2,n}/\sqrt{2} + a'_{2,n}}{I_n + n'_{1,n}/\sqrt{2} + a'_{1,n}}\right) \tag{23}$$

is a noise-like phase fluctuation on the interferer's phase θ_n, and is due to the noise and spread spectrum signal. The terms $n'_{1,n}$, $n'_{2,n}$, $a'_{1,n}$, and $a'_{2,n}$ are in-phase and quadrature components of the noise and spread spectrum signal with respect to the interference phase θ_n, i.e.,

$$n'_{1,n} = n_{1,n}\cos(\theta_n) + n_{2,n}\sin(\theta_n) \tag{24}$$

$$n'_{2,n} = n_{2,n}\cos(\theta_n) - n_{1,n}\sin(\theta_n) \tag{25}$$

$$a'_{1,n} = a_n\cos(\theta_n) \tag{26}$$

$$a'_{2,n} = -a_n\sin(\theta_n). \tag{27}$$

If the interference is of constant envelope and $I \gg (s_n + n_n)$, then Eq. (23) simplifies to

$$\phi_{u,n} \approx \left(\frac{n'_{2,n}/\sqrt{2} + a'_{2,n}}{I}\right). \tag{28}$$

The output of the limiter/bandpass filter is [11]

$$bp_n = \frac{4A'}{\pi}\cos(\omega_0 n + \theta_n + \phi_{u,n}), \tag{29}$$

where A' is the limiter's output level. This signal is redefined as (letting $A' = \sqrt{2}\pi/4$ for convenience)

$$bp_n = \sqrt{2}\cos[\omega_0 n + \theta_n + \phi_{u,n}]. \tag{30}$$

It should be noted that for large interference-to-noise ratios in which the interference is of constant envelope, $\phi_{u,n}$ in Eq. (30) is approximately Gaussian [11]. The sampled signal in Eq. (30) is what is processed by the Kalman filter, which estimates the phase θ_n of the interference. The phase estimate is denoted as $\hat{\theta}_{n|n-1}$.

The interference estimator shown in Fig. 1 is detailed in Fig. 7. The Kalman algorithm from Fig. 4 produces the VCO signal defined in Eq. (21) and shifted by $\pi/2$ radians. This signal is

$$\hat{y}_n = \sqrt{2}\cos(\omega_0 n + \hat{\theta}_{n|n-1}) \tag{31}$$

and can be used as a basis for estimating a sampled version of the envelope of $i(t)$ (i.e., I_n in Eq. (6)). The output of the first multiplier is a baseband term and is, using Eq. (7),

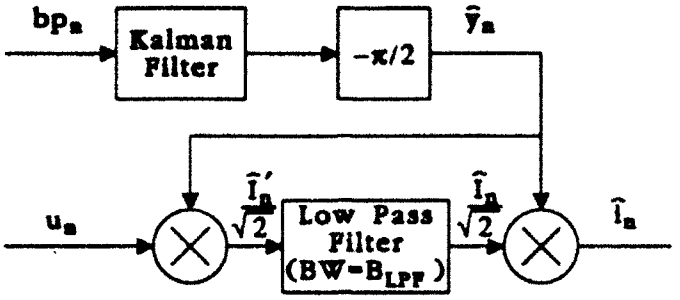

Figure 7: Block diagram of the interference estimator.

excluding the $\sqrt{2}$ factor,

$$\begin{aligned} \hat{I}'_n &= I_n \cos(\theta_n - \hat{\theta}_{n|n-1}) \\ &+ n_n \cos(\omega_0 n + \hat{\theta}_{n|n-1}) + a_n \cos(\hat{\theta}_{n|n-1}) \\ &+ a_n \cos(2\omega_0 n + \hat{\theta}_{n|n-1}). \end{aligned} \tag{32}$$

Equation (32) consists of four terms: the first term is related to the desired envelope of the interference; the second is approximately Gaussian baseband noise [10]; and the third and fourth terms are noise-like terms emanating from the spread spectrum signal. The fourth term, because of the sampling rate conditions discussed in [1], is essentially filtered out by the low pass filter of bandwidth $B_{LPF} < 0.50$ Hz and, therefore, will be ignored in the baseband simulations to be discussed in the next section. The term $\hat{I}'_n/\sqrt{2}$ is filtered, resulting in the estimate of the interference envelope, $\hat{I}_n/\sqrt{2}$. Combining this with $\hat{y}_n$ in Eq. (31) and shown in Fig. 7 yields the estimate of the interference

$$\hat{i}_n = \hat{I}_n \cos(\omega_0 n + \hat{\theta}_{n|n-1}), \tag{33}$$

which is subtracted from u_n as illustrated in Fig. 1.

5.0 THEORETICAL BIT ERROR RATE PERFORMANCE

For the development of the theoretical bit error rate expression, one can refer to Figs. 1 and 7. In Fig. 1, the error signal e_n prior to despreading (but following decimation and sign reversal) will be used. This error is defined as

$$\begin{aligned} e_n &= u_n - \hat{i}_n \\ &= s_n + n_n + i_n - \hat{i}_n \end{aligned}$$

$$= \quad s_n + n_n + \Delta i_n. \tag{34}$$

In Eq. (34) the signal s_n has been set equal to a_n which was defined following Eq. (7), and n_n has been set equal to the in-phase-noise term $n_{1,n}$. It is assumed that the interferer is of constant envelope and that the baseband representation of it is used, i.e.,

$$i_n = I\cos(\theta_n). \tag{35}$$

Furthermore, it is generated using the interference model in Fig 3.

From Fig. 7, the interference estimate $\hat{i}_n$ is

$$\hat{i}_n = \hat{I}\cos(\hat{\theta}_{n|n-1}) \tag{36}$$

where

$$\hat{I} = \left[I\cos(\epsilon_n) + \sqrt{E_c/2}n_{B,n} + s_n\cos(\hat{\theta}_{n|n-1})\right] * h_{LPF,n}. \tag{37}$$

In Eq. (37),

$$\epsilon_n = \theta_n - \hat{\theta}_{n|n-1} \tag{38}$$

and $n_{B,n}$ is a baseband noise term defined as

$$n_{B,n} = n_{1,n}\cos(\hat{\theta}_{n|n-1}) + n_{2,n}\sin(\hat{\theta}_{n|n-1}) \tag{39}$$

where the terms $n_{1,n}$ and $n_{2,n}$ are the in-phase and quadrature noise terms of n_n prior to decimation. Furthermore, $h_{LPF,n}$ is the impulse response of the low pass filter in Fig. 7 and $*$ is the convolution operator. With E_c of unit energy and Eq. (37) substituted into Eq. (36), the interference estimate becomes

$$\begin{aligned}\hat{i}_n \quad &= \quad \left\{\left[I\cos(\epsilon_n)\right] * h_{LPF,n}\right\}\cos(\hat{\theta}_{n|n-1}) + \\ &+ \quad \left\{\left[n_{B,n}/\sqrt{2} + s_n\cos(\hat{\theta}_{n|n-1})\right] * h_{LPF,n}\right\}\cos(\hat{\theta}_{n|n-1}).\end{aligned} \tag{40}$$

This interference estimate consists of two terms: (a) the first term is closely related to the interference in Eq. (35); (b) the second term is low pass filtered noise and signal, modulated by an estimate of the phase variations of the interference.

The first term, because it is a function of $\hat{\theta}_{n|n-1}$, which in turn is a function of the past data, is uncorrelated with the signal and noise, s_n and n_n. The same cannot be said about the second term, since it contains noise and signal terms at time n. However, the degree of cross-correlation will be a function of the bandwidth of the interference

characteristics and the low pass filter with impulse response $h_{LPF,n}$.

To illustrate the point, consider a simple example which is close to the worst case situation in which the low pass filter in Fig. 7 is of a rectangular shape of bandwidth $B_{LPF} = 0.50$ Hz. Furthermore, assume the interference has a very narrow bandwidth, close to a single tone, offset from the spread spectrum signal by a small amount δf Hz. If, for illustrative purposes, the phase-noise is considered to be negligible, then $\hat{\theta}_{n|n-1} \approx 2\pi\delta f n$, so that the signal term in Eq. (32), $a_n \cos\hat{\theta}_{n|n-1}$, after low pass filtering, will have a truncated spectrum offset from 0 Hz by $\pm\delta f$ Hz. This new signal, when mixed by $\hat{y}_n$ in Fig. 7, will result in a shifting back to baseband of the truncated spectrum, with significant signal energy in the neighbourhood of 0 Hz, i.e., in the region

$$-B_{LPF} + \delta f < f < B_{LPF} - \delta f.$$

After decimation this baseband term becomes

$$\{[a_n \cos(\hat{\theta}_{n|n-1})] * h_{LPF}]\} \cos(\hat{\theta}_{n|n-1})$$

where, as noted earlier, $a_n = s_n$. One can see that the amount of signal energy in the region around 0 Hz diminishes as B_{LPF} decreases from its maximum value of 0.50 Hz and as δf increases. A similar situation occurs with the noise.

Therefore, consider the case where the bandwidth B_{LPF} is sufficiently small so that the second term in Eq. (40) is weakly correlated with s_n and n_n. With these simplifications, the signal-to-noise ratio at the output of the despreader can be approximated by

$$\begin{aligned} SNR_o &= \frac{L^2}{LN_0/2 + LE\{\Delta i_n^2\}} \\ &= \frac{L}{N_0/2 + E\{\Delta i_n^2\}} \end{aligned} \tag{41}$$

where the derivation of Eq. (41) is similar to the derivation of Eq. (59) in [5] for the linear prediction case. In deriving Eq. (41), it has been assumed that Δi_n is weakly correlated with s_n and n_n for the reasons stated above, that s_n is uncorrelated with n_n, and that the chips of the PN code over a bit interval are uncorrelated. Finally, because the energy per chip was set to unity, and the number of chips per bit is L, the energy per bit is $E_b = L$. Thus, for no residual interference Δi, Eq. (41) reduces to the standard equation for BPSK signals in AWGN.

If it is assumed that the noise plus residual interference have Gaussian statistics

[12], the bit error rate can be represented by

$$P_b = \frac{1}{2} erfc\sqrt{SNR_o/2}, \tag{42}$$

where $erfc(x)$ is the complementary error function. As an example of the Gaussian assumption, a histogram of the residual interference resulting from an FM interferer is illustrated in Fig. 8 along with a normal curve. As can be seen, the fit is quite good for the most part. In fact, for this example, the number of degrees of freedom was 100, and $\chi^2 = 114$ for a 10% rejection probability. However, as pointed out in Section 3.2.1 in relation to the stable tone for high signal-to-noise ratios at the output of the despreader, performance will be governed by the behaviour of the density function in its tail-region. This behaviour in turn will also be a function of the operating conditions of the excisor.

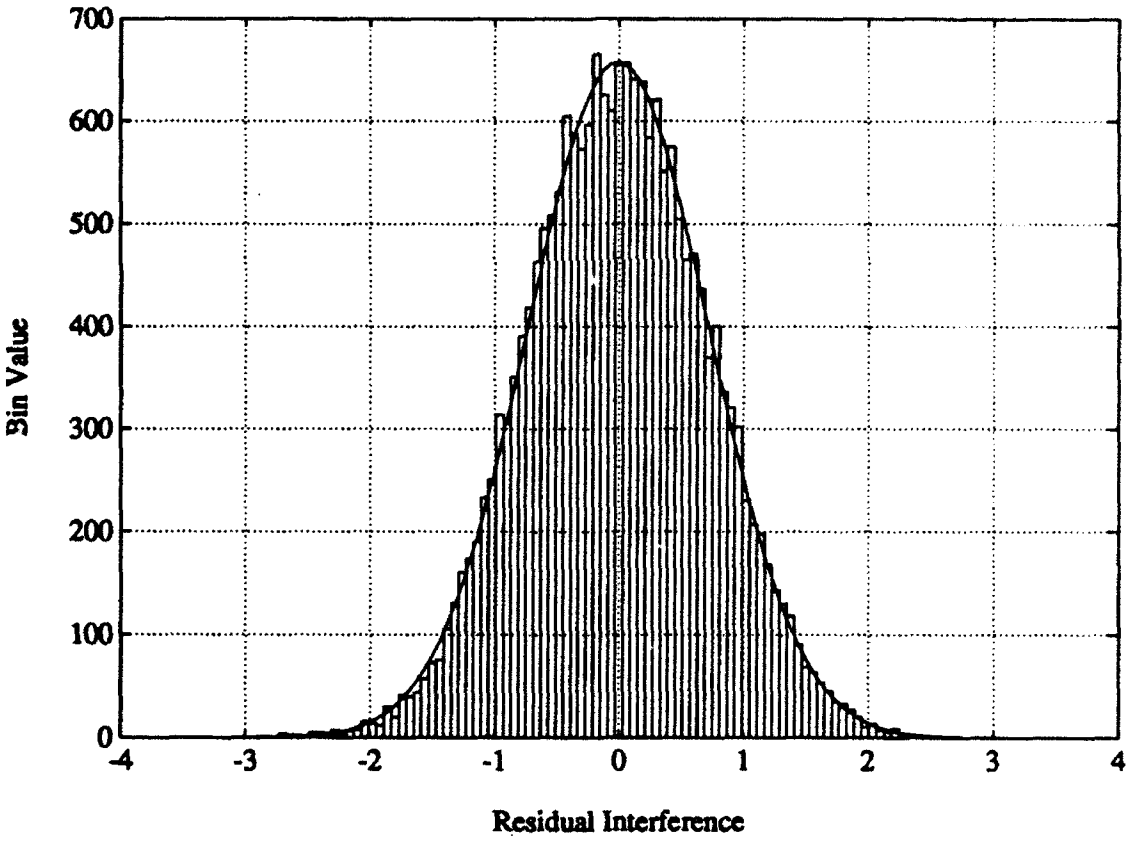

Figure 8: Histogram of residual interference for the case when the interference is FM, generated by the state-space model in Fig. 3.

The next step is to develop an expression for $E\{\Delta i_n^2\}$ in Eq. (41) for later substitution into Eq. (42). The residual interference is, using Eqs. (35) and (40),

$$\begin{aligned}\Delta i_n &= I\Big\{1 - \Big[\cos(\epsilon_n) * h_{LPF,n}\Big]\cos(\epsilon_n) \\ &+ 1/I\Big(\Big[1/\sqrt{2}n_{B,n} + s_n\cos(\hat{\theta}_{n|n-1})\Big] * h_{LPF,n}\Big)\cos(\epsilon_n)\Big\}\cos(\theta_n) \\ &+ I\Big\{\Big[\cos(\epsilon_n) * h_{LPF,n}\Big]\sin(\epsilon_n) \\ &+ 1/I\Big(\Big[1/\sqrt{2}n_{B,n} + s_n\cos(\hat{\theta}_{n|n-1})\Big] * h_{LPF,n}\Big)\sin(\epsilon_n)\Big\}\sin(\theta_n). \qquad (43)\end{aligned}$$

Equation (43) shows that the residual interference consists of two terms, one related to the in-phase interference component and one related to the quadrature component.

Consider the in-phase term first. If the term $[\cos(\epsilon_n) * h_{LPF,n}]\cos(\epsilon_n)$ is approximated by $\cos^2(\epsilon_n)$ (the worst case situation in which the low pass filter has no effect on the phase-noise term), and if $\epsilon_n \ll 1$ (see Fig. 9 for an example), and $\cos(\epsilon_n) \approx 1$, then

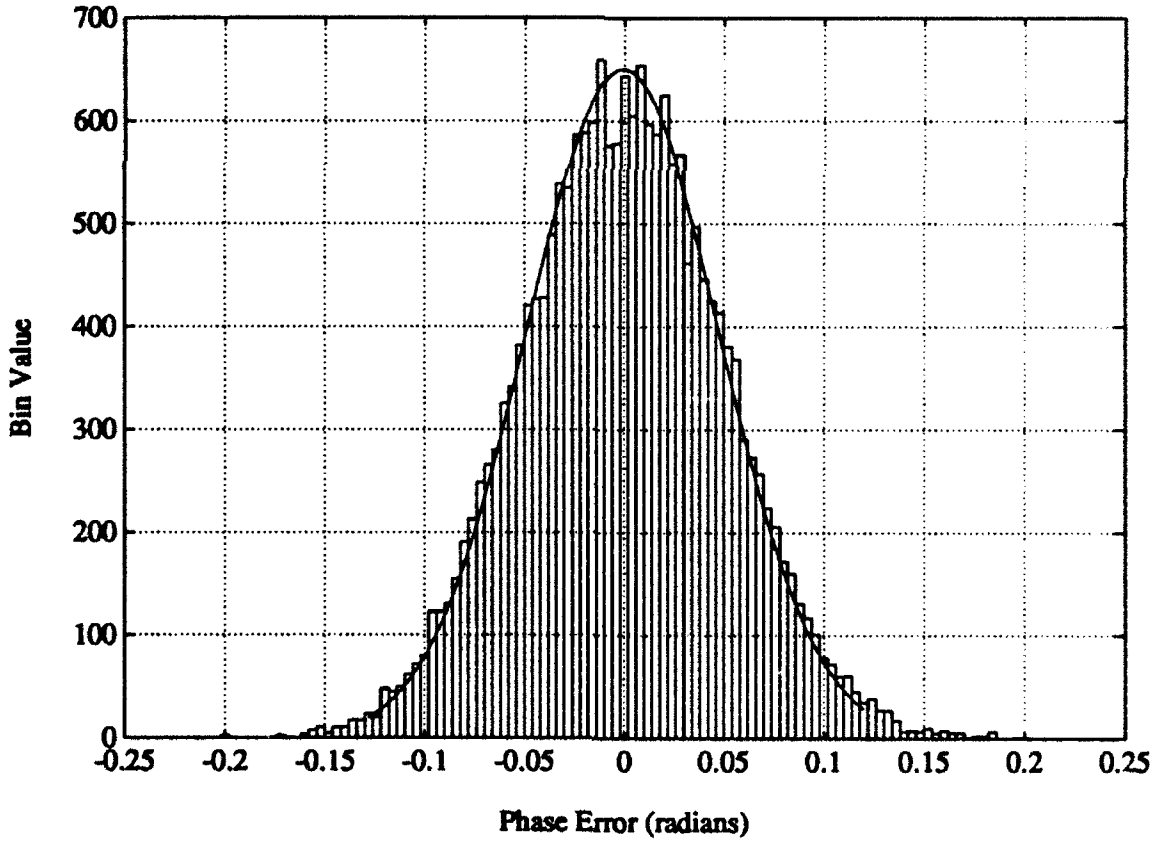

Figure 9: Histogram of phase error ϵ_n.

the in-phase term can be approximated by

$$\Delta i_{I,n} \approx \left\{ I\epsilon_n^2 + \left[1/\sqrt{2} n_{B,n} + s_n \cos(\hat{\theta}_{n|n-1}) \right] * h_{LPF,n} \right\} \cos(\theta_n). \tag{44}$$

Equation (44) contains two noise terms, one due to the phase-noise (a second order effect), and one due to additive noise and signal which have been low pass filtered.

Now consider the quadrature term in Eq. (43). Using the approximation $\sin(\epsilon_n) \approx \epsilon_n$,

$$\Delta i_{Q,n} \approx \left\{ I\epsilon_n + \left(\left[1/\sqrt{2} n_{B,n} + s_n \cos(\hat{\theta}_{n|n-1}) \right] * h_{LPF,n} \right) \epsilon_n \right\} \sin(\theta_n). \tag{45}$$

Equation (45) shows that the residual interference in the quadrature direction consists of a first order phase-noise term and a combination of the additive noise and phase-noise (a second order effect). Considering Eqs. (44) and (45) one might intuitively conclude that the second order terms can be neglected for low phase-noise cases, and that the residual interference is therefore dominated by the noise and signal terms in Eq. (44) and the phase-noise term in Eq. (45). Furthermore, for a narrow bandwidth low pass filter of bandwidth B_{LPF}, it is conceivable that the quadrature term in Eq. (45) could dominate. This was in fact pointed out in Fig. 9 of [8] for the swept tone case when little difference in performance was achieved between $B_{LPF} = 0.05$ Hz and 0.025 Hz.

If it is assumed that ϵ_n is weakly correlated with

$$\left[1/\sqrt{2} n_{B,n} + s_n \cos(\hat{\theta}_{n|n-1}) \right] * h_{LPF,n}$$

in Eqs. (44) and (45), the residual interference power in the in-phase direction is

$$E\{\Delta i_{I,n}^2\} \approx (I^2/2) E\{\epsilon_n^4\} + P_{sn}/2 \tag{46}$$

where P_{sn} is the power of the signal- and noise-related terms in Eq. (44), i.e., the power in

$$[1/\sqrt{2} n_{B,n} + s_n \cos(\hat{\theta}_{n|n-1})] * h_{LPF,n}.$$

Similarly, the residual interference power in the quadrature component is

$$\begin{aligned} E\{\Delta i_{Q,n}^2\} &\approx (I^2/2) E\{\epsilon_n^2\} + (1/2) E\{\epsilon_n^2\} P_{sn} \\ &\approx (I^2/2) E\{\epsilon_n^2\} \end{aligned} \tag{47}$$

where it has been assumed that $I^2 \gg P_{sn}$. Finally, the residual interference power is,

using Eqs. (46) and (47),

$$\begin{aligned} E\{\Delta i^2\} &\approx E\{\Delta i_{I,n}^2\} + E\{\Delta i_{Q,n}^2\} \\ &\approx (I^2/2)E\{\epsilon_n^2\} + P_{sn}/2 + (I^2/2)E\{\epsilon_n^4\} \\ &\approx (I^2/2)E\{\epsilon_n^2\} + P_{sn}/2 \end{aligned} \tag{48}$$

where the term $(I^2/2)E\{\epsilon_n^4\}$ can be neglected under low phase-noise conditions. It should be noted that P_{sn} can also be neglected when the low pass filter bandwidth B_{LPF} is small.

Expressions for $E\{\epsilon_n^2\}$, $E\{\epsilon_n^4\}$, and P_{sn} in Eq. (48) will now be determined. If the Kalman filter has reached steady state and its linear form is assumed [6], then the filtered phase-noise of Eq. (28) is

$$\epsilon_n \approx \phi_{u,n} * h_{Kal,n} \tag{49}$$

where $h_{Kal,n}$ is the steady state impulse response of the optimum filter. Expanding Eq. (49),

$$\begin{aligned} \epsilon_n &= 1/I\left[(n'_{2,n}/\sqrt{2}) * h_{Kal,n} + [s_n \sin(\theta_n)] * h_{Kal,n}\right] \\ &= N_n/I + S_n/I \end{aligned} \tag{50}$$

where

$$N_n = (n'_{2,n}/\sqrt{2}) * h_{Kal,n} \tag{51}$$

and

$$S_n = [s_n \sin(\theta_n)] * h_{Kal,n}. \tag{52}$$

Since s_n and $n'_{2,n}$ from Eq. (25) are uncorrelated, S_n and N_n are uncorrelated. It will be assumed, furthermore, that N_n and S_n are Gaussian random variables. Figure 10 illustrates the histogram of the term $n'_{2,n}/(\sqrt{2}I)$ in Eq. (51) before Kalman filtering and Fig. 11 illustrates the histogram of the same term after filtering. Observe that in both cases the statistics indicate a definite Gaussian feature. Figure 12 illustrates the histogram of $s_n \sin(\theta_n)$ in Eq. (52) before filtering, and Fig. 13 shows the same term after filtering. The input term in Fig. 13 is far from Gaussian, whereas the output term has a reasonable Gaussian feature.

If the mean-squared values of the output phase-noise terms N_n/I and S_n/I from Eq. (50) are combined, they can be represented by $V_{\tilde{x}_{11,\infty}}$, the steady state phase-noise variance at the output of the Kalman filter, the performance curves of which were

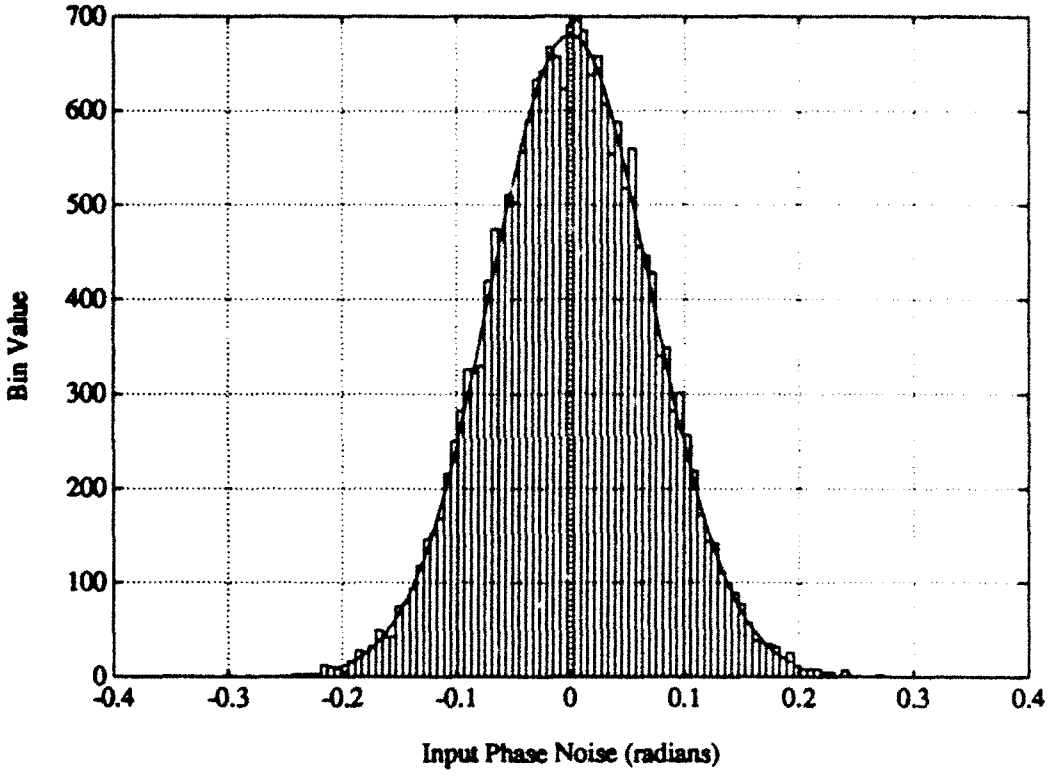

Figure 10: Histogram of $n'_{2,n}/(\sqrt{2}I)$ from Eq. (51) before Kalman filtering.

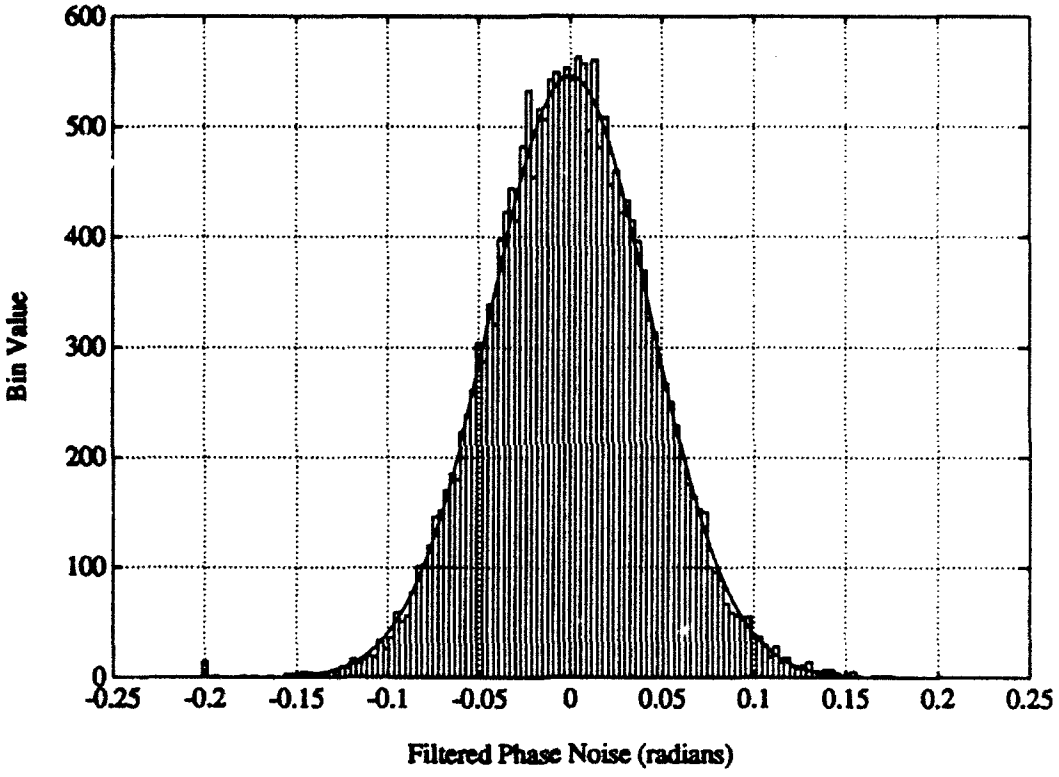

Figure 11: Histogram of $n'_{2,n}/(\sqrt{2}I) * h_{Kal,n}$ from Eq. (51).

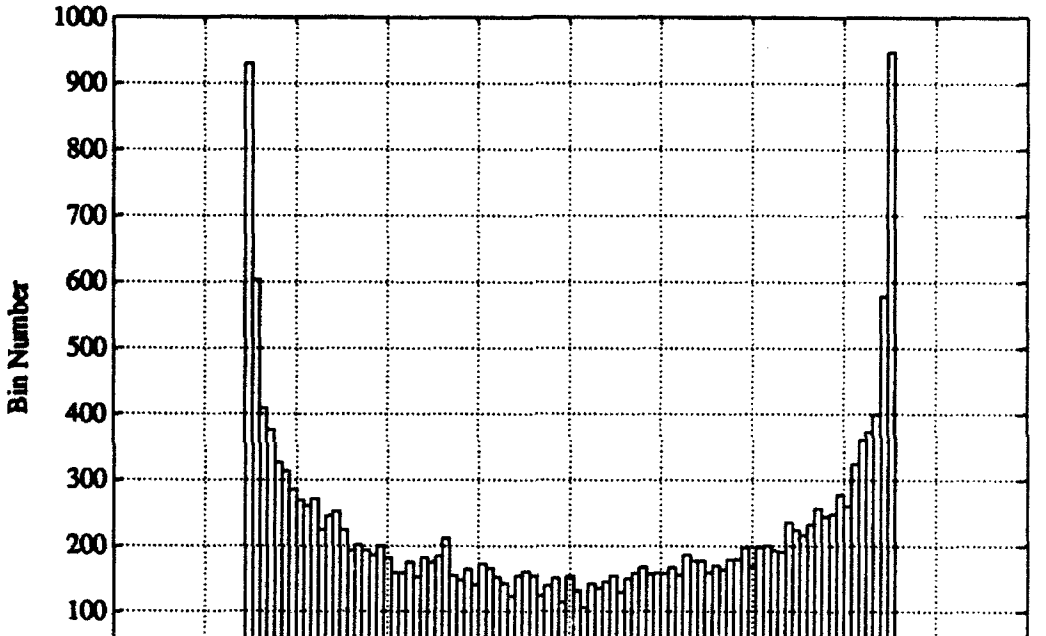

Figure 12: Histogram of the signal term $s_n \cos(\theta_n)$ from Eq. (52) before Kalman filtering.

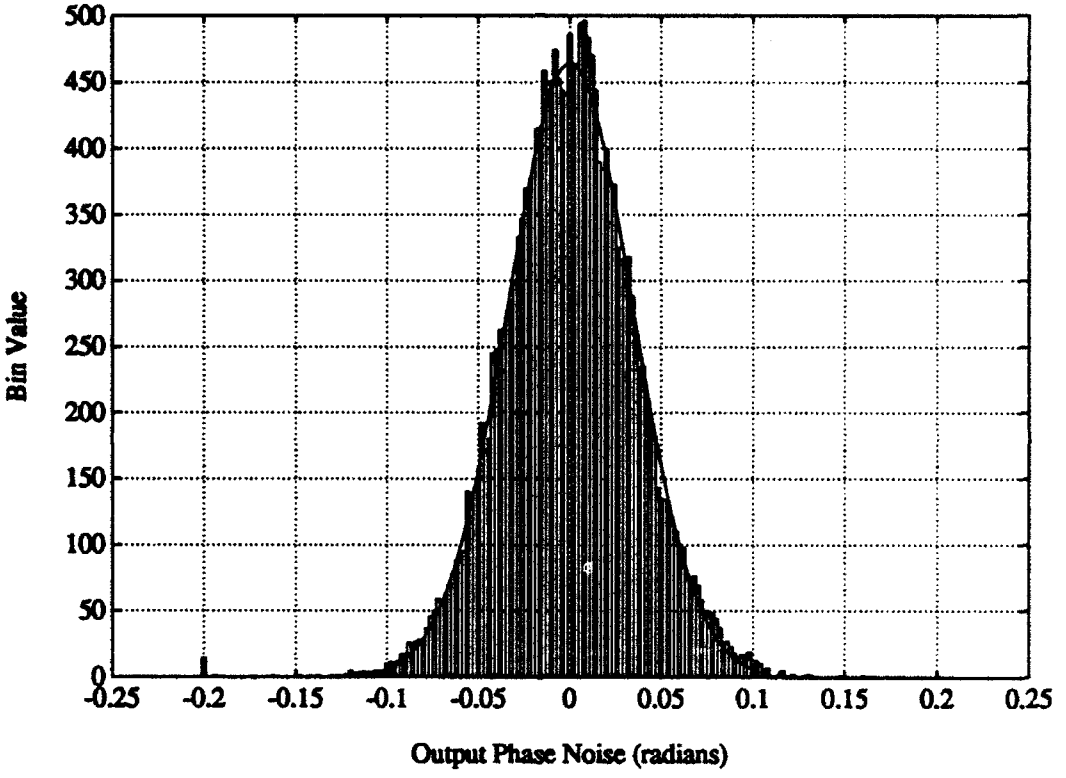

Figure 13: Histogram of the signal term $s_n \cos(\theta_n) * h_{Kal,n}$ from Eq. (52).

illustrated in Fig. 5. With this Gaussian assumption then,

$$E\{\epsilon_n^2\} = V_{\tilde{z}_{11,\infty}} \tag{53}$$

and

$$E\{\epsilon_n^4\} = 3V_{\tilde{z}_{11,\infty}}^2. \tag{54}$$

Finally, to complete the derivation of an expression for $E\{\Delta i_n^2\}$ in Eq. (41), an expression for P_{sn} from Eq. (48) must be determined. Recall that P_{sn} is the power in the term $[1/\sqrt{2}n_{B,n} + s_n \cos(\hat{\theta}_{n|n-1})] * h_{LPF,n}$ in Eq. (43). If the terms $n'_{B,n}/\sqrt{2}$ and $s_n \cos(\hat{\theta}_{n|n-1})$ from Eq. (39) are assumed to be flat over the lowpass filter bandwidth with power spectral densities $N_0/2$ and 0.5 respectively (refer to Fig. 14 for an example), then

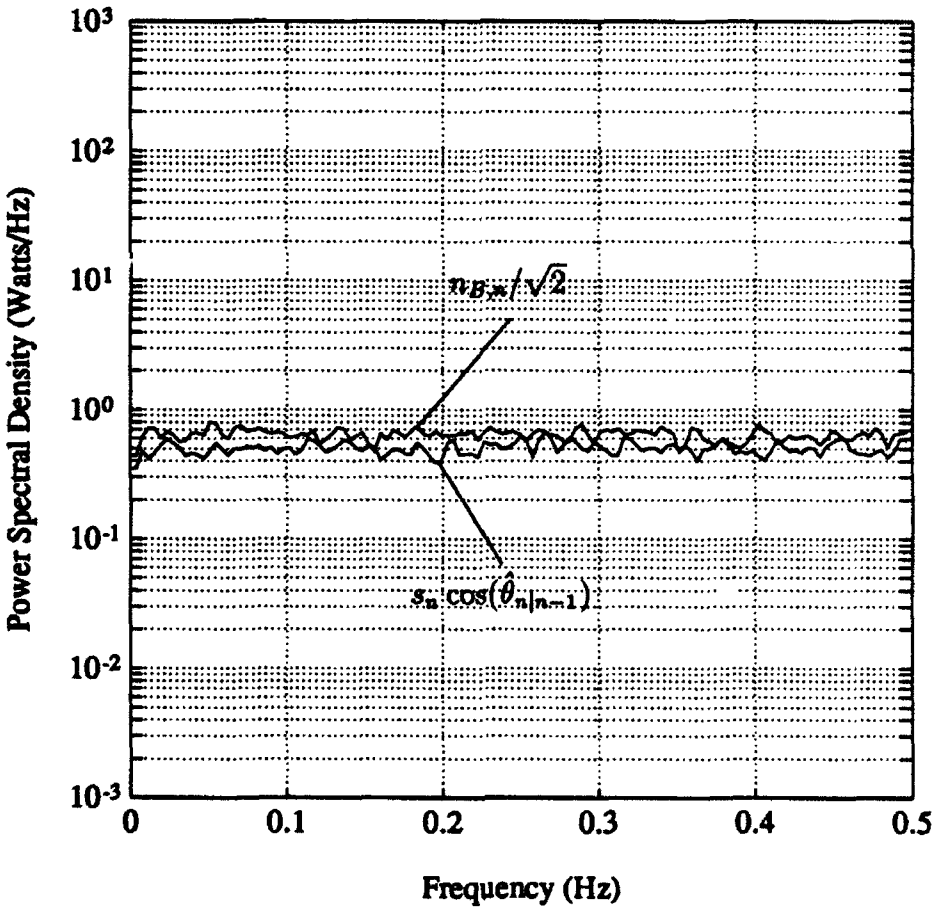

Figure 14: Power spectral density of the signal term $s_n \cos(\hat{\theta}_{n|n-1})$ and noise term $n_{B,n}/\sqrt{2}$ for the case $E_b/N_0 = 12$ dB, $(E_b = L = 20)$.

$$P_{sn} \approx B_{LPF}(N_0/2 + 0.5). \tag{55}$$

With these approximations,

$$E\{\Delta i^2\} \approx (I^2/2)(3V^2_{\tilde{x}_{11,\infty}} + V_{\tilde{x}_{11,\infty}}) + B_{LPF}(N_0/2 + 0.5)/2 \tag{56}$$

and

$$SNR_o = \frac{L}{N_0/2 + (I^2/2)(3V^2_{\tilde{x}_{11,\infty}} + V_{\tilde{x}_{11,\infty}}) + B_{LPF}(N_0/2 + 0.5)/2}. \tag{57}$$

Examples of the accuracy of the bit error rate formula as represented by Eq. (42) using Eq. (57), are presented next. The interference considered is of constant envelope and of the FM type generated from the interference model in Fig. 3. The interference-to-signal ratio was set at 20 dB and the bandwidth expansion factor β was 400. The processing gain was L=20 (also equal to E_b). The values for E_b/N_0 ranged from 0 to 12 dB. The modified Kalman algorithm was used in the simulations. In addition, the performance curves illustrated in Fig. 6 for the filter form of the modified Kalman algorithm were used to obtain the values for $V_{\tilde{x}_{11,\infty}}$ for use in Eq. (57). Finally, the 3 dB bandwidth, B_{LPF}, of a 4-pole low pass Butterworth filter was used in Eq. (57).

The power spectrum of the signal, noise, plus interference is illustrated in Fig. 15. This was determined using the Welch algorithm for two cases, i.e., $E_b/N_0 = 0$ dB and 12 dB.

The bit error rate performance is illustrated in Figs. 16 to 19. The low pass filter bandwidth B_{LPF} ranged from 0.1 Hz to 0.4 Hz in steps of 0.1 Hz. For $B_{LPF} = 0.1$ and 0.2 Hz (Figs. 16 and 17), there is reasonable agreement between theory and the computer simulations. The difference starts to manifest itself for larger values of B_{LPF}, i.e., 0.3 and 0.4 Hz (Figs. 18 and 19). This is to be expected, as it was pointed out in the development of Eq. (57) that the correlation between the low pass filtered signal and noise terms, (i.e., the term

$$\{[n_{B,n}/\sqrt{2} + s_n \cos(\hat{\theta}_{n|n-1})] * h_{LPF,n}\} \cos(\hat{\theta}_{n|n-1})$$

in Eqs. (44) and (45)) and $s_n + n_n$ would increase with increasing B_{LPF}. This phenomenon is illustrated in Figs. 20 and 21 for $B_{LPF} = 0.1$ and 0.4 Hz, respectively.

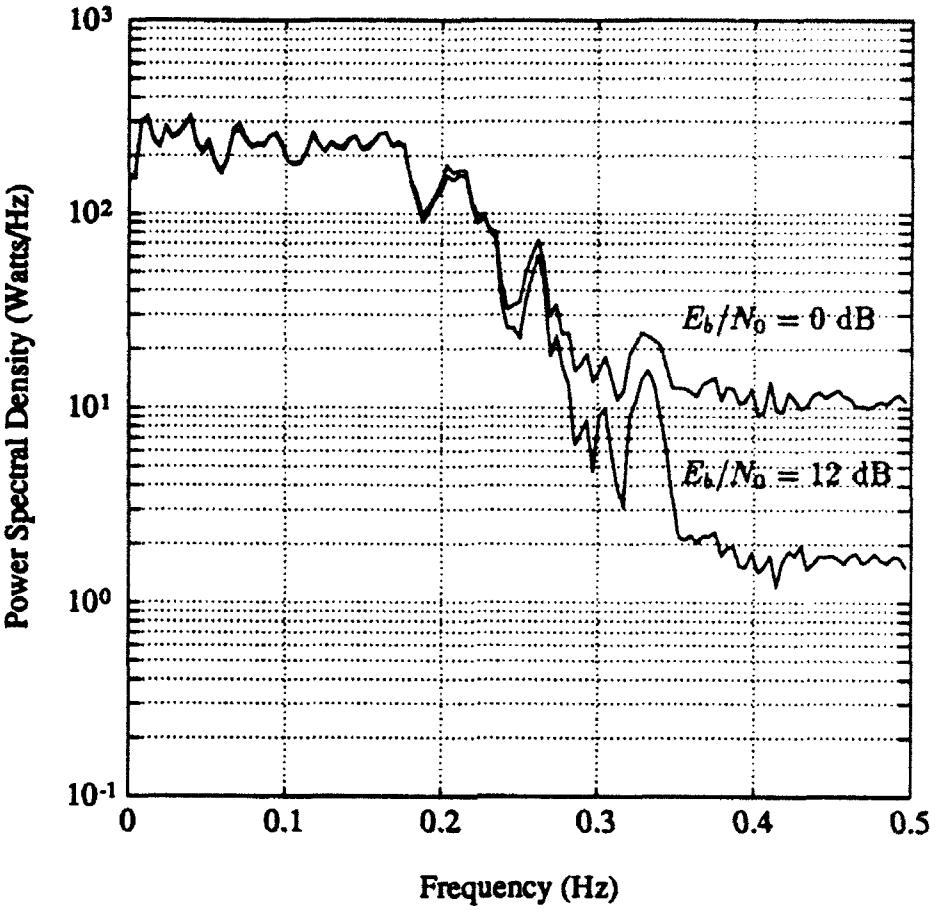

Figure 15: Power spectral density of $s_n + n_n + i_n$ for $E_b/N_0 = 0$ dB and $E_b/N_0 = 12$ dB.

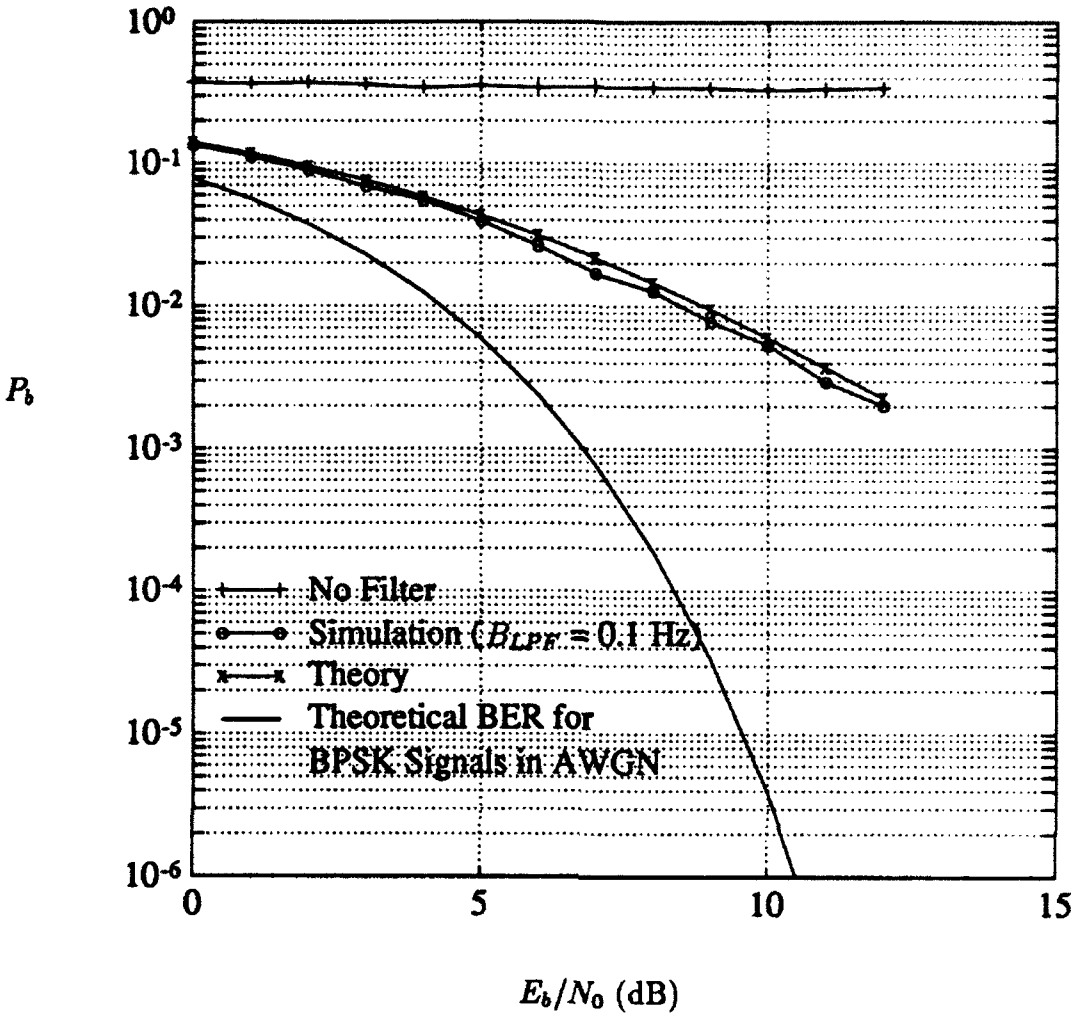

Figure 16: Comparison of the bit error rate performance of the modified Kalman filter algorithm with Eq. (42) for the case of $B_{LPF} = 0.1$ Hz.

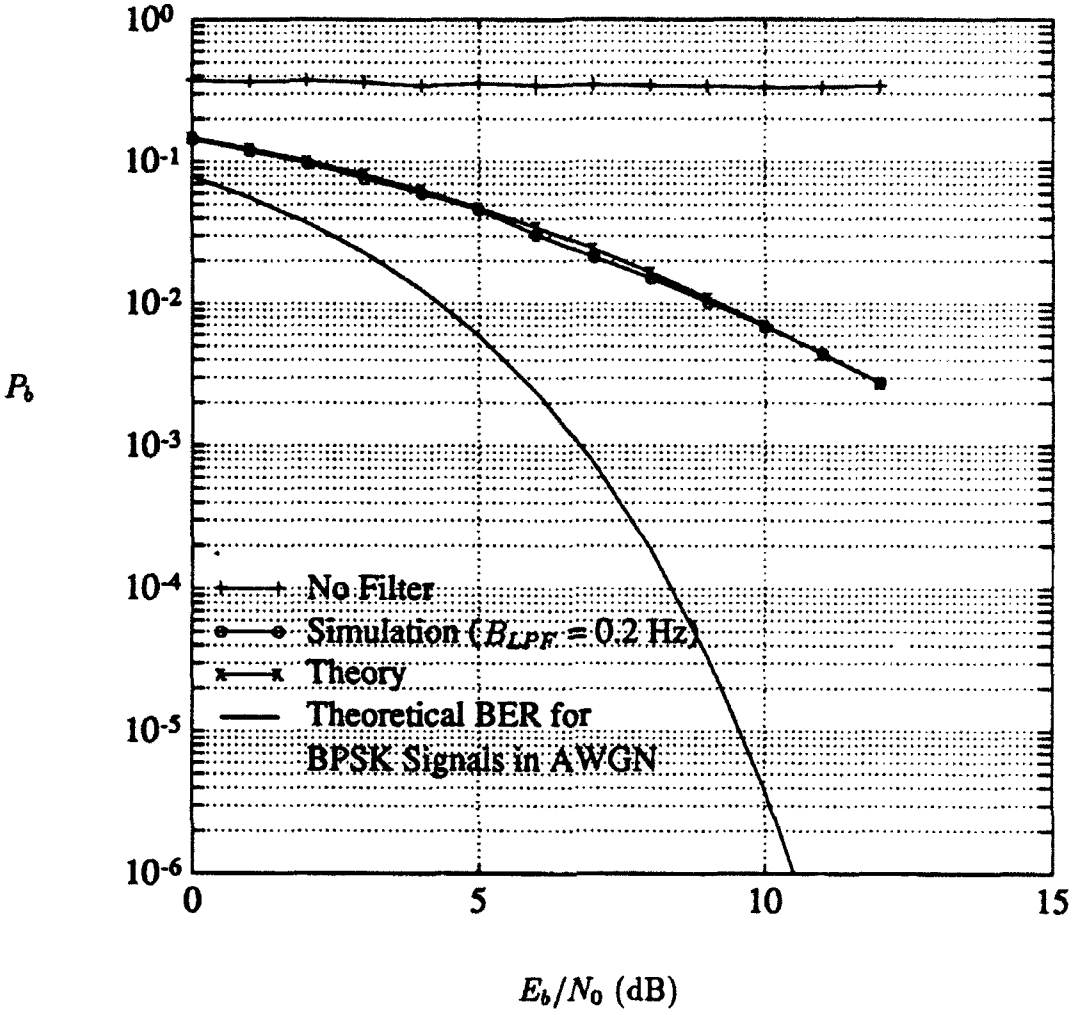

Figure 17: Comparison of the bit error rate performance of the modified Kalman filter algorithm with Eq. (42) for the case of $B_{LPF} = 0.2$ Hz.

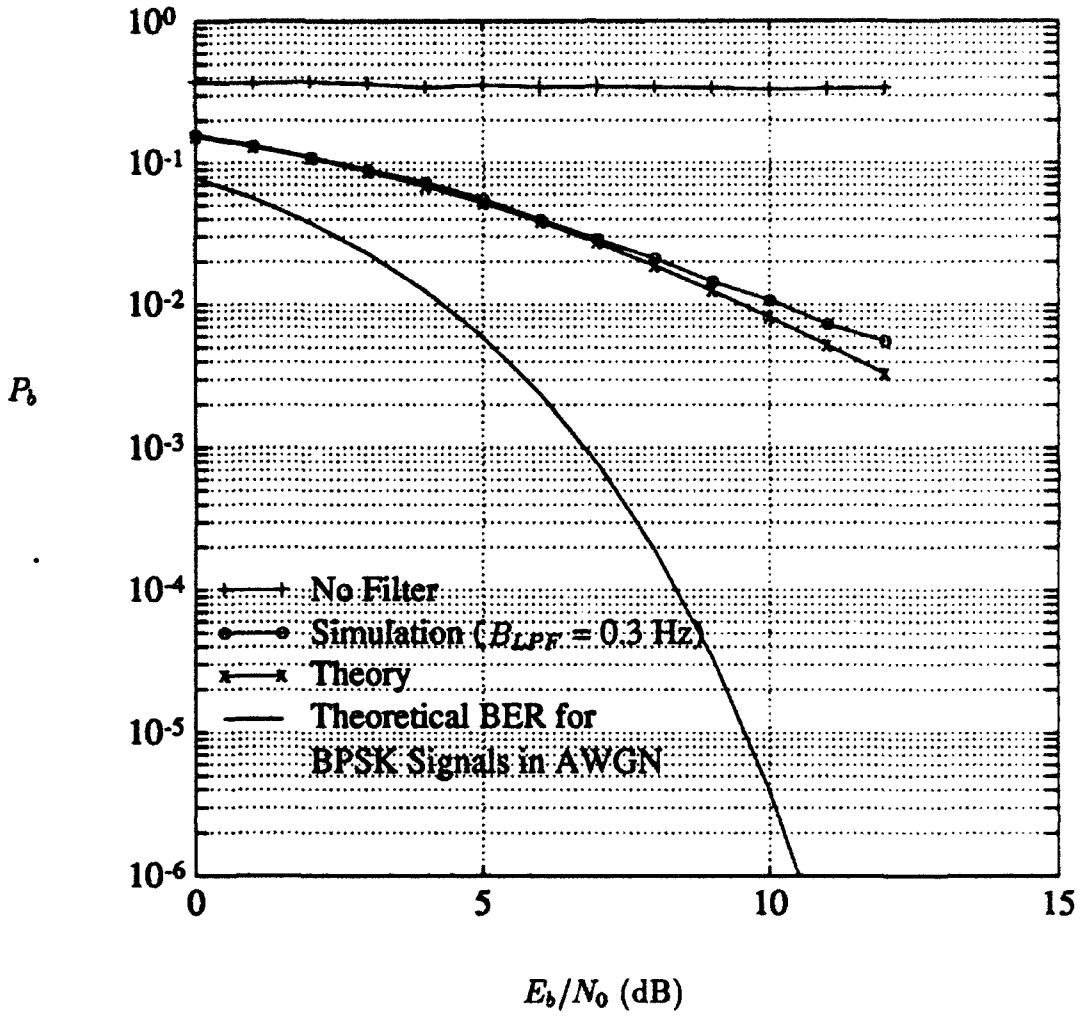

Figure 18: Comparison of the bit error rate performance of the modified Kalman filter algorithm with Eq. (42) for the case of $B_{LPF} = 0.3$ Hz.

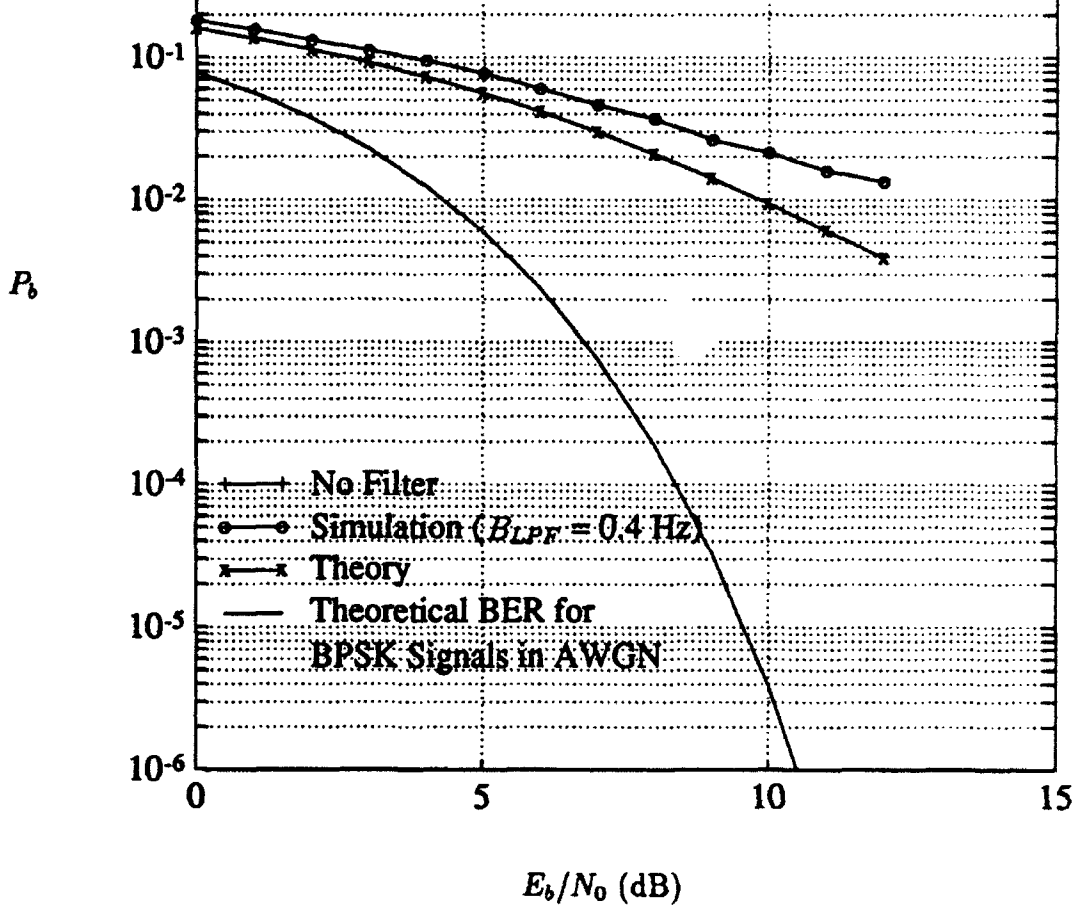

Figure 19: Comparison of the bit error rate performance of the modified Kalman filter algorithm with Eq. (42) for the case of $B_{LPF} = 0.4$ Hz.

Figure 20 shows very little distortion of the signal at the output of the excisor, i.e.,

$$s_n - \{[s_n \cos(\hat{\theta}_{n|n-1})] * h_{LPF,n}\} \cos(\hat{\theta}_{n|n-1})$$

for $B_{LPF} = 0.1$ Hz before the PN correlator in Fig. 1. The curve referring to

$$\{[s_n \cos(\hat{\theta}_{n|n-1})] * h_{LPF,n}\} \cos(\hat{\theta}_{n|n-1}),$$

is approximately 10 dB lower in power in the vicinity of 0 Hz. Figure 21, which corresponds to $B_{LPF} = 0.4$ Hz, shows some distortion of the signal. In fact, the difference in power was 20% or 1 dB. Similar distortion phenomena also occurred with the noise term

$$\{n'_{B,n} * h_{LPF,n}\} \cos(\hat{\theta}_{n|n-1})$$

for the two lowpass filter bandwidths, although these are not illustrated here.

Finally, Fig. 22 shows an example of the power spectral density of the interference, i_n, interference estimate,

$$\{[I \cos(\epsilon_n)] * h_{LPF,n}\} \cos(\hat{\theta}_{n|n-1})$$

(which excludes the signal and noise term effects), and the residual interference,

$$i_n - \{[I \cos(\epsilon_n)] * h_{LPF,n}\} \cos(\hat{\theta}_{n|n-1}),$$

for $E_b/N_0 = 12$ dB and $B_{LPF} = 0.1$ Hz. The degree of interference suppression for this example was 17.38 dB, and the mean-squared value of the residual interference was 1.83. For $B_{LPF} = 0.4$ Hz, the degree of interference suppression and mean-squared value of the residual interference were almost identical to that for $B_{LPF} = 0.1$ Hz, i.e., 17.39 dB and 1.82. This leads one to the conclusion that residual interference was not a factor in the reasons for the difference between the bit error rate curves of $B_{LPF} = 0.4$ Hz, but that it was due to other factors such as signal and noise distortion and the violation of several assumptions which were made in the development of the bit error rate formula in Eq. (42), the primary one being that B_{LPF} be significantly less than 0.50 Hz.

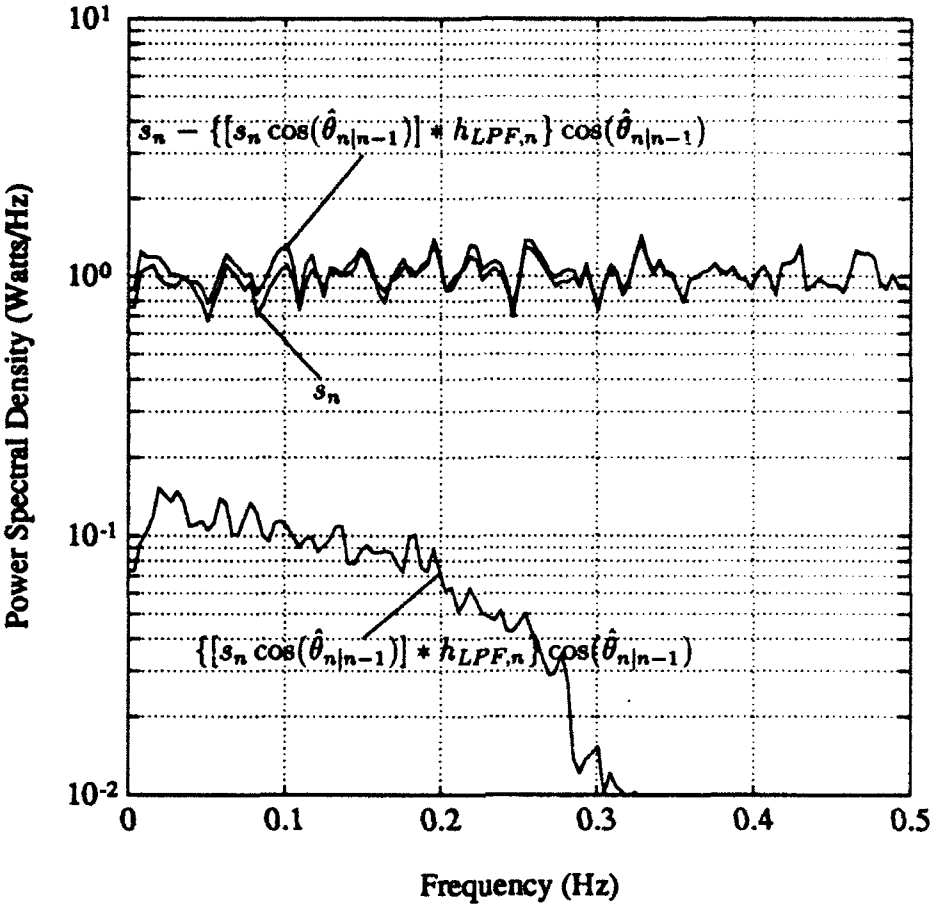

Figure 20: Power spectral density of signal s_n, the filtered signal term $\{[s_n \cos(\hat{\theta}_{n|n-1})] * h_{LPF,n}\} \cos(\hat{\theta}_{n|n-1})$ and the residual signal term $s_n - \{[s_n \cos(\hat{\theta}_{n|n-1})] * h_{LPF,n}\} \cos(\hat{\theta}_{n|n-1})$. The bandwidth of the lowpass filter is $B_{LPF} = 0.1$ Hz.

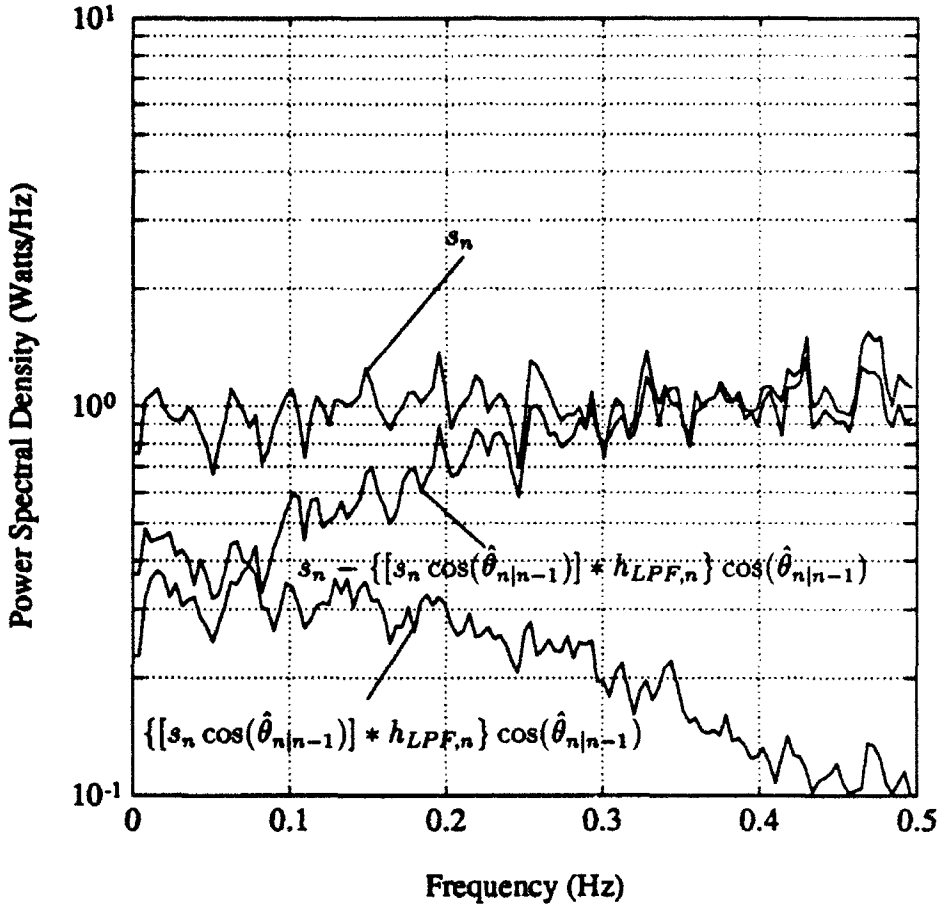

Figure 21: Power spectral density of signal s_n, the filtered signal term $\{[s_n \cos(\hat{\theta}_{n|n-1})] * h_{LPF,n}\} \cos(\hat{\theta}_{n|n-1})$, and the residual signal term $s_n - \{[s_n \cos(\hat{\theta}_{n|n-1})] * h_{LPF,n}\} \cos(\hat{\theta}_{n|n-1})$. The bandwidth of the lowpass filter is $B_{LPF} = 0.4$ Hz.

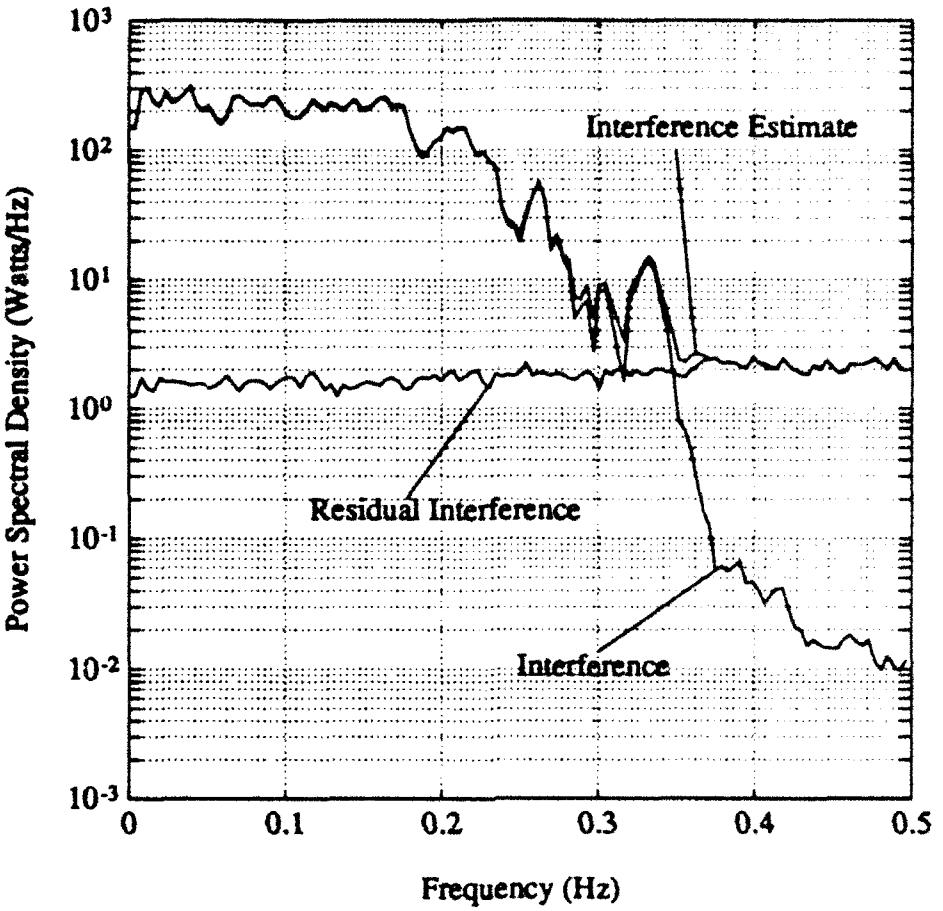

Figure 22: Power spectral density of interference i_n, the interference estimate $\{[I\cos(\epsilon_n)] * h_{LPF,n}\}\cos(\theta_{n|n-1})$, and the residual term $i_n - \{[I\cos(\epsilon_n)] * h_{LPF,n}\}\cos(\theta_{n|n-1})$. The bandwidth of the lowpass filter is $B_{LPF} = 0.1$ Hz.

6.0 CONCLUSIONS

A bit error rate expression for the Kalman filter excisor has been developed based on several assumptions which were elaborated upon. The interference in this case was of the FM-type generated by the state space model on which the Kalman filter algorithm was derived. It was shown and illustrated that theory agrees well with simulation as long as the bandwidth B_{LPF} of the low pass filter used to determine the envelope of the interference is much less than the sampling rate. It was also shown that the interference estimate at the input to the interference canceller will have significant cross-correlation with the signal, leading to some cancellation of the spread spectrum signal, if the bandwidth B_{LPF}

is large relative to the sampling rate.

For constant envelope interference, or interferers whose envelopes vary slowly with time, the approach taken in this report will work well. However, for narrowband Gaussian noise it will not, this being due to the sudden phase changes when the envelope goes to zero and the resulting temporary loss of lock of the Kalman filter. The effect would be an increase in residual interference which could not be modelled accurately as Gaussian. More work in this area is required.

REFERENCES

[1] D. R. Polk and S. C. Gupta, "Quasi–optimum digital phase–locked loops," *IEEE Transactions on Communications*, vol. 21, pp. 75–82, January 1973.

[2] F. M. Hsu and A. A. Giordano, "Digital whitening techniques for improving spread spectrum communications performance in the presence of narrowband jamming and interference," *IEEE Transactions on Communications*, vol. 26, pp. 209–216, February 1978.

[3] J. W. Ketchum and J. G. Proakis, "Adaptive algorithms for estimating and suppressing narrowband interference in PN spread-spectrum systems," *IEEE Transactions on Communications*, vol. 30, pp. 913–924, May 1982.

[4] L. B. Milstein, "Interference rejection techniques in spread spectrum communications," *Proceedings of the IEEE*, vol. 76, pp. 657–671, June 1988.

[5] B. W. Kozminchuk, "Excision techniques in direct sequence spread spectrum communication systems," Technical Report 1047, Defence Research Establishment Ottawa, Ottawa, Ontario, Canada, K1A 0Z4, 1990.

[6] B. W. Kozminchuk, "Kalman filter-based architectures for interference excision," Technical Report 1118, Defence Research Establishment Ottawa, Ottawa, Ontario, Canada, K1A 0Z4, 1991.

[7] C. N. Kelly and S. C. Gupta, "The digital phase-locked loop as a near-optimum FM demodulator," *IEEE Transactions on Communications*, vol. 20, pp. 406–411, June 1972.

[8] B. W. Kozminchuk, "A comparison of recursive least squares and Kalman filtering excisors for swept tone interference," Technical Note 92-14, Defence Research Establishment Ottawa, Ottawa, Ontario, Canada, K1A 0Z4, 1992.

[9] A. P. Sage and J. L. Melsa, *Estimation Theory with Applications to Communications and Control.* New York: McGraw-Hill, 1971.

[10] H. L. Van Trees, *Detection, Estimation, and Modulation–Part 2: Nonlinear Modulation Theory.* New York: John Wiley and Sons, 1971.

[11] A. Blanchard, *Phase-Locked Loops.* New York: John Wiley and Sons, 1976.

REFERENCES

[12] J. W. Ketchum, "Decision feedback techniques for interference cancellation in PN spread-spectrum communication systems," in *IEEE Miltitary Communications Conference*, pp. 39.5.1–39.5.5, October 1984.

DOCUMENT CONTROL DATA

(Security classification of title, body of abstract and indexing annotation must be entered when the overall document is classified)

1. ORIGINATOR (the name and address of the organization preparing the document. Organizations for whom the document was prepared, e.g. Establishment sponsoring a contractor's report, or tasking agency, are entered in section 8.)

DEFENCE RESEARCH ESTABLISHMENT OTTAWA
NATIONAL DEFENCE
SHIRLEY BAY, OTTAWA, ONTARIO K1A 0K2 CANADA

2. SECURITY CLASSIFICATION (overall security classification of the document including special warning terms if applicable)

UNCLASSIFIED

3. TITLE (the complete document title as indicated on the title page. Its classification should be indicated by the appropriate abbreviation (S,C or U) in parentheses after the title.)

THEORETICAL BIT ERROR RATE PERFORMANCE OF THE KALMAN FILTER EXCISOR FOR FM INTERFERENCE (U)

4. AUTHORS (Last name, first name, middle initial)

KOZMINCHUK, BRIAN W.

5. DATE OF PUBLICATION (month and year of publication of document)

NOVEMBER 1992

6a. NO. OF PAGES (total containing information. Include Annexes, Appendices, etc.)

48

6b. NO. OF REFS (total cited in document)

12

7. DESCRIPTIVE NOTES (the category of the document, e.g. technical report, technical note or memorandum. If appropriate, enter the type of report, e.g. interim, progress, summary, annual or final. Give the inclusive dates when a specific reporting period is covered.)

DREO REPORT

8. SPONSORING ACTIVITY (the name of the department project office or laboratory sponsoring the research and development. Include the address.)

DEFENCE RESEARCH ESTABLISHMENT OTTAWA
NATIONAL DEFENCE
SHIRLEY BAY, OTTAWA, ONTARIO K1A 0K2 CANADA

9a. PROJECT OR GRANT NO. (if appropriate, the applicable research and development project or grant number under which the document was written. Please specify whether project or grant)

041LK11

9b. CONTRACT NO. (if appropriate, the applicable number under which the document was written)

10a. ORIGINATOR'S DOCUMENT NUMBER (the official document number by which the document is identified by the originating activity. This number must be unique to this document.)

DREO REPORT 1163

10b. OTHER DOCUMENT NOS. (Any other numbers which may be assigned this document either by the originator or by the sponsor)

11. DOCUMENT AVAILABILITY (any limitations on further dissemination of the document, other than those imposed by security classification)

(X) Unlimited distribution
( ) Distribution limited to defence departments and defence contractors; further distribution only as approved
( ) Distribution limited to defence departments and Canadian defence contractors; further distribution only as approved
( ) Distribution limited to government departments and agencies; further distribution only as approved
( ) Distribution limited to defence departments; further distribution only as approved
( ) Other (please specify):

12. DOCUMENT ANNOUNCEMENT (any limitation to the bibliographic announcement of this document. This will normally correspond to the Document Availabilty (11). However, where further distribution (beyond the audience specified in 11) is possible, a wider announcement audience may be selected.)

13. ABSTRACT (a brief and factual summary of the document. It may also appear elsewhere in the body of the document itself. It is highly desirable that the abstract of classified documents be unclassified. Each paragraph of the abstract shall begin with an indication of the security classification of the information in the paragraph (unless the document itself is unclassified) represented as (S) (C), or (U). It is not necessary to include here abstracts in both offical languages unless the text is bilingual).

(U) This technical report develops a theoretical bit error rate expression for a Kalman filtering technique that is used for filtering narrowband interferers out of direct sequence spread spectrum signals. The approach is based on the digital phase-locked loop Kalman filter and is close to optimum in so far as demodulating an FM-type of interferer. Because the interference is assumed to be much stronger than either the signal or noise, the Kalman filter locks onto the interference and produces estimates of its phase and envelope. Several assumptions are made in the development of the theoretical bit error rate expression and these are expanded upon. It is shown and illustrated that theory agrees well with simulation as long as the bandwidth of the low pass filter used to determine the envelope of the interference is much less than the sampling rate, otherwise the interference estimate at the input to the interference canceller will have significant cross-correlation with the signal, leading to some cancellation of the spread spectrum signal.

14. KEYWORDS, DESCRIPTORS or IDENTIFIERS (technically meaningful terms or short phrases that characterize a document and could be helpful in cataloguing the document. They should be selected so that no security classification is required. Identifiers, such as equipment model designation, trade name, military project code name, geographic location may also be included. If possible keywords should be selected from a published thesaurus. e.g. Thesaurus of Engineering and Scientific Terms (TEST) and that thesaurus-identified. If it is not possible to select indexing terms which are Unclassified, the classification of each should be indicated as with the title.)

KALMAN FILTER
MODULATION
INTERFERENCE SUPPRESSION
EXCISION
SPREAD SPECTRUM
DIRECT SEQUENCE
ELECTRONIC SUPPORT MEASURES